TAPERED ROLLER BEARING BALLSCREW SUPPORT SYSTEM

by

Douglas H. Smith

Submitted to the Department of Mechanical Engineering
in Partial Fulfillment of the Requirements for the Degrees of

BACHELOR OF SCIENCE IN MECHANICAL ENGINEERING

and

MASTER OF SCIENCE IN MECHANICAL ENGINEERING

at the
MASSACHUSETTS INSTITUTE OF TECHNOLOGY
February 1994

Signature of Author. . . . . .
Department of Mechanical Engineering

Certified by . . . . . .
Alexander H. Slocum, Associate Professor of Mechanical Engineering
Thesis Advisor

Accepted by . . . . . .
Ain A. Sonin, Professor of Mechanical Engineering
Chairman, Graduate School Committee

Tapered Roller Bearing Ballscrew Support System

by

Douglas H. Smith

Submitted to the Department of Mechanical Engineering on February 14, 1994 in partial fulfillment of the requirements for the Degrees of Bachelor of Science in Mechanical Engineering and Master of Science in Mechanical Engineering.

Abstract

A comparison of tapered roller bearings and angular contact ball bearings as the support bearings in a machine-tool ballscrew application was performed. The application requirements of high axial stiffness, low running torque, space minimization, and cost effectiveness were used to design a two-row tapered roller bearing solution to compare against a widely used three-row 'triplex' angular contact ball bearing solution. Theoretical axial stiffness and torque analyses of both bearing packages were challenged and found to be sound models of the physical systems. Incorporating the theoretical characteristics of the ballscrew and ballnut stiffnesses and torques, predictions were made and tested on an assembled machine-tool axis for both bearing types.

The worst case system stiffness when using the triplex angular contact ball bearings as the ballscrew support bearings was 1.439×10^6 lb/in compared to 1.355×10^6 lb/in when using the two-row tapered roller bearing solution. In both cases the experimental results were within 2.5% of the theoretical predictions.

The worst case system torque when using the triplex angular contact ball bearings was 51 in-lb at start-up and 47 in-lb at constant speed compared to 80 in-lb for the two-row tapered roller bearing solution at start-up and 75 in-lb at constant speed. The experimental torque results fell within 10% of the theoretical predictions.

Thesis Supervisor: Alexander H. Slocum
Title: Associate Professor of Mechanical Engineering

Acknowledgments

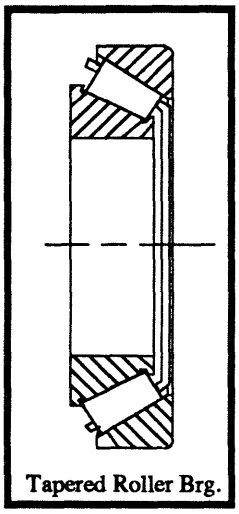
Tapered Roller Brg.

Immense enthusiasm and support was provided for this project and I would like to take the opportunity to thank the individuals who I was fortunate to come into contact with during my work. Without their assistance this project would never have materialized and I am ever indebted to their selfless dedication.

The Timken Company

Ravi Bhatia, Chief Engineer - Mobile Industrial
Marvin Debevec, Sr. NPH Associate
Mike Dreher, Process Equipment Analyst
Rosendo Fuquen, Mgr. NDE/Sensor Technology
Richard Johns, Mgr. Precision Brg. Business - NPH
Larry Laps, Supv. Engineer. - Mfg. Engineer
Pat Linet, Mgr. Product Testing
Doug Link, Sr. Prod. Dev. Technician
David Mintz, Sr. Development Engineer
Peter Orvos, Gen. Mgr. Prod. Dev. - Bearings
David Slicker, Sr. Prod. Dev. Specialist
Dave Swihart, Prod. Dev. Analyst
R. Davis Webb, Mgr. Prototype Manufacuring
Marc Weston, Mkt. Mgr. Aero/Military Mkts.
Dave Walters, Sr. NPH Associate

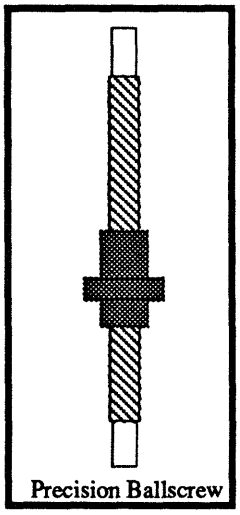
Precision Ballscrew

Cincinnati Milacron, Inc.

Joe Dykes, Project Engineer
Gary Haas, Sr. Project Engineer
Richard Kurless, Chief Engineer - Fountain Inn
Barrington McCullough, Engineering Intern
John McCullough, Mgr. Building Services
Bob Sickler, Project Engr - Fountain Inn

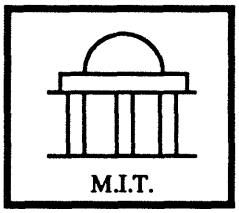
M.I.T.

Massachusetts Institute of Technology

To Professor Alex Slocum I give my greatest thanks. The time and effort spent on this and other projects will be eternally appreciated and remembered. Opportunities come and go, but friendships last forever.

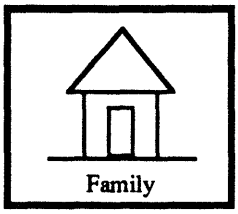
Family

Personal Thanks

To my wife Stefanie, my parents Doug and Patricia, and my brothers Dan and Scott; your loving support and guidance has kept me on the straight and narrow and has taught me the true meaning of family.

Table of Contents

1.0

Introduction.

The necessity of evolution continues to push the envelope of machine-tool design. A globally competitive marketplace has driven the machine-tool industry into the arms of those capable of harnessing every ounce of performance from their machines. Designs must be better, faster, and cheaper if they are to impact the already clouded machine-tool arena. The next generation of machine-tools are being designed for faster axis actuation with greater positioning accuracy under increasingly hostile conditions. This calls for enhancement of the ballscrew actuation systems that are commonly used to propel carriages along their respective axes.

1.1 Background.

A large percentage of machine-tools employ ballscrew driven axes because of their ability to accurately transmit rotational motion into linear motion[1]. A typical ballscrew axis can be seen in Figure 1-1.

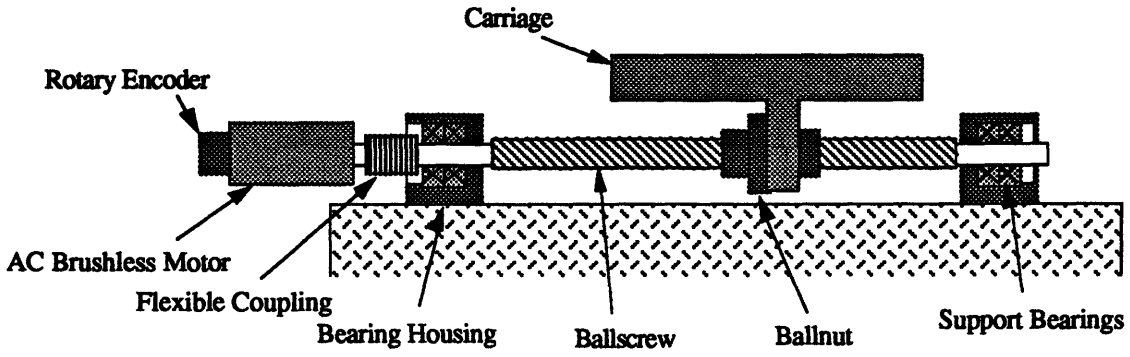

Figure 1-1. Typical Ballscrew Driven Axis.

Linear actuation is accomplished by the ballnut which rides back and forth along the ballscrew. The motion arises from the fact that the ballnut is constrained in all directions except along the axis of the ballscrew. Within the ballnut are tracks of recirculating steel balls that come into rolling contact with the precision thread along the ballscrew. When the ballscrew is rotated the ballnut traverses along the axis. With the thread direction in Figure 1-1, if the ballscrew is viewed from the motor end, and the ballscrew is turned clockwise, the ballnut and carriage will traverse towards the motor.

The carriage is supported by linear guides which provide two key features allowing the operation of the ballscrew system. First, the linear guides allow free, uninhibited travel in the direction of the ballscrew axis. Secondly, they bear the load components that are oriented perpendicular to the axis of the ballscrew. Therefore, when a ballscrew is properly aligned, it will only experience the thrust components of the applied loads.

---

[1] See also: A. H. Slocum. Precision Machine Design. Prentice Hall, New Jersey. 1992 pp. 719-727

The ballscrew is able to rotate as a result of the support bearings that are located on both ends. These bearings are critical components and are responsible for a variety of functions. They must maintain precise rotational motion with minimal rotational resistance while handling the axial loads that the ballscrew is subjected to during operation.

A typical drive system incorporates a servomotor that is closed-loop controlled by a rotary encoder. The servomotor is affixed to the ballscrew via a flexible coupling that allows rotational motion to be transmitted while allowing for some axial misalignment due to mounting tolerances.

To achieve the best operating conditions possible, each component of the ballscrew axes must be optimized. The ballscrew, by virtue of its geometry and nature of operation represents the limiting component. Hence, much work has been done to improve ballscrew efficiency. Several design options involve surface finish, helical thread angle, and tolerancing that directly affect performance. An additional area of optimization involves the mounting of the ballscrew in the machine-tool application.

Ballscrews are stretched in many applications. This tensile mounting configuration minimizes the effects of actuator thermal growth by 'burying' the thermal strain with an induced elastic strain. As Section 4.0 will detail, stretching the ballscrew also improves the operating characteristics of the ballscrew. However, by applying a stretch to the ballscrew, the support bearings are forced to carry much higher axial loads causing additional problems. First, several rows of ball bearings must be stacked to achieve the necessary stiffnesses and load carrying capabilities of the ballscrew axes, but this is not a cost effective solution as more parts and more space are necessary. Secondly, the sensitivity of the bearings to varying operating conditions is a concern. Thermal growth of the ballscrew and machine in general cause the loading conditions to vary across the bearings, influencing their operating characteristics. The resulting change in axial stiffness affects the positioning accuracy, repeatability, and controllability of the ballscrew driven axis.

Tapered roller bearings are being investigated as support bearings for ballscrew driven systems as they offer excellent axial load carrying capabilities and maintain a constant axial stiffness throughout their loading range.

1.2 Bearing Overview.

The following section introduces the geometries and critical features associated with angular contact ball bearings and tapered roller bearings. Also introduced is the concept of bearing preload.

1.2.1 Angular Contact Ball Bearing Nomenclature.

The basic components of the angular contact ball bearing can be seen in Figure 1-1. The bearing is composed of inner and outer raceways, balls, and a retainer. The retainer that is used to keep the balls from rubbing against one another is not depicted in Figure 1-1 as retainer styles can vary depending upon the application.

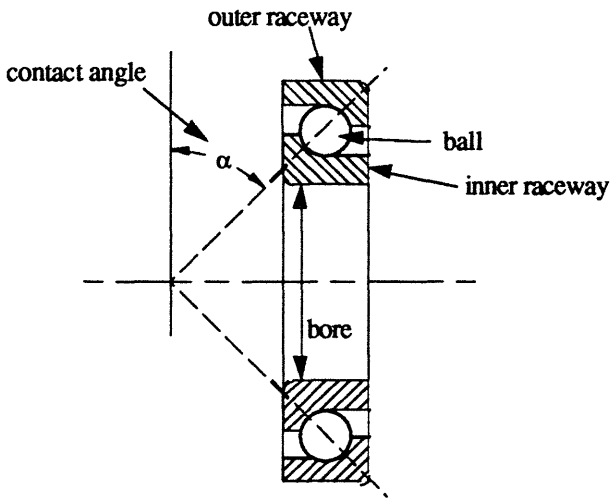

Figure 1-1. Angular Contact Ball Bearing Nomenclature.

The nominal 60° angular contact ball bearing used in ballscrew support applications is billed as an anti-friction bearing. Through geometry, rolling motion is created between the balls and the raceways. By establishing point contact between the balls and the raceways, lines of contact can be drawn that extend through these contact points converging upon a single location along the rotational axis of the ball bearing. These bearings have been adopted for use in ballscrew support applications by virtue of their low operating torque, appreciable axial load carrying capability, and axial stiffness when stacked in multiple row arrangements.

1.2.2 Tapered Roller Bearing Nomenclature.

Figure 1-2 shows the cross section of a tapered roller bearing. The cage is not shown in the figure but it is an integral part of the geometry of the tapered roller bearing. The cage prevents the rollers from coming into contact with one another as they roll around the raceways.

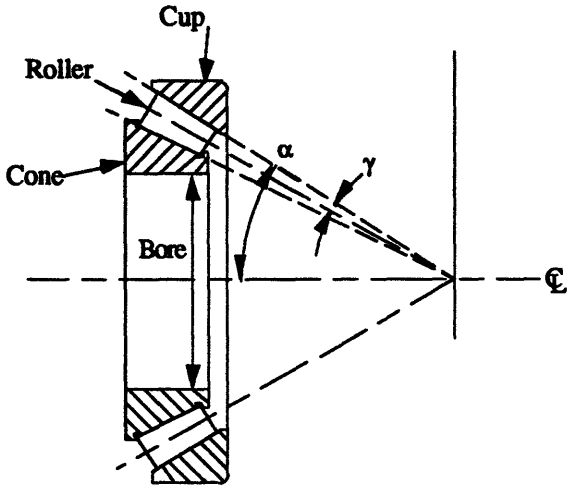

Figure 1-2. Tapered Roller Bearing Nomenclature.

Figure 1-2 illustrates the basis behind the anti-friction nature of the tapered roller bearing. The rollers rotate around the raceways in true rolling motion as the individual apices of the rollers converge at one point along the rotational axis of the bearing. This creates a line of contact between the rollers, the cup, and the cone allowing for very large axial load carrying capabilities and stable axial stiffnesses which will be detailed in Section 3.1. This bearing is very robust and well suited to aggressive applications requiring high axial stiffnesses due to the large contact area between the rolling elements and the raceways.

As there is a greater contact area between the rollers and the raceways than there is for the ball bearing under point contact, more effort is required to rotate the tapered roller bearing. Ballscrew actuators are typically low-speed, intermittent motion applications. Therefore, torque related concerns are minimized. Further torque minimization can be attained for the tapered roller bearing through proper profiling, enhanced surface finishes, and proper lubrication. Rotational resistance will be explained further in Sections 2.3 and 3.3.

1.2.3 Bearing Preload.

'Preload' can be thought of as a load that is instilled upon the bearing prior to operation. Preloading eliminates any floating ball or roller conditions, assuring that the rolling elements are in contact with both the inner and outer raceways. This load is commonly set by the bearing manufacturer who grinds the contacting faces of stacked bearings such that a gap is created between the bearings when they are pressed onto a shaft or into a housing. An example of which can be seen in the mounting configuration seen in Figure 1-3.

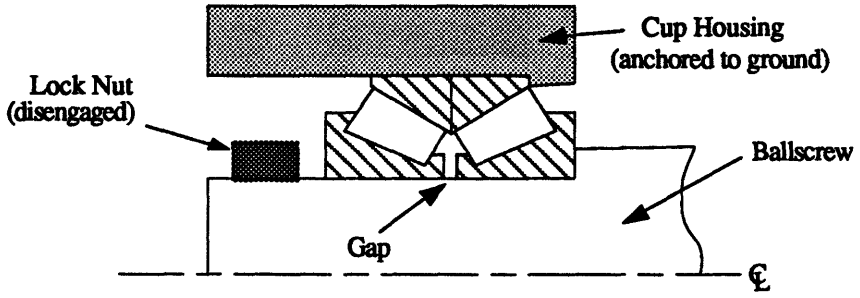

Figure 1-3. Illustration of the Gap Used to Set System Preload.

This gap is subsequently squeezed shut by the application of a nut on the end of the shaft or some form of a follower bolted onto the housing. By squeezing the gap shut until the ground surfaces come into contact, preload is applied to the system. There are many means of setting preloads. Some of these methods include the use of shims, ground spacers, springs, and over or under-sized balls or rollers. Figure 1-4 shows the resulting compression of the bearings due to the approach of a locknut.

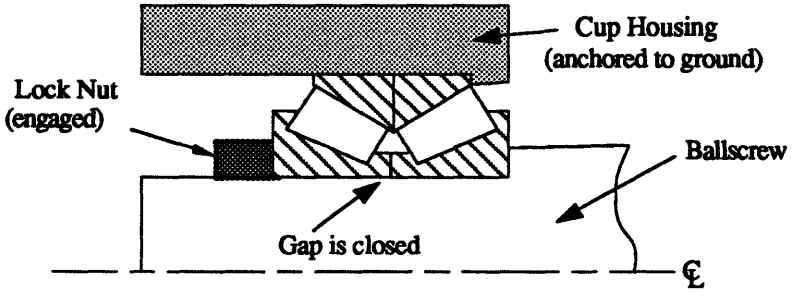

Figure 1-4. Illustration of Preloaded System.

Any load that the system sees during operation is called an applied load and is in addition to the preload already within the system. It will be shown in Section 2.0 how the contact angle across the rolling elements in angular contact ball bearings changes in relation to the axial load. It is therefore important to realize that the preload within the system contributes to the total load and effects the contact angle determining the axial deflection and axial stiffness. An illustration of the effect of preload on the load deflection curve of an angular contact ball bearing can be seen in Figure 1-5.

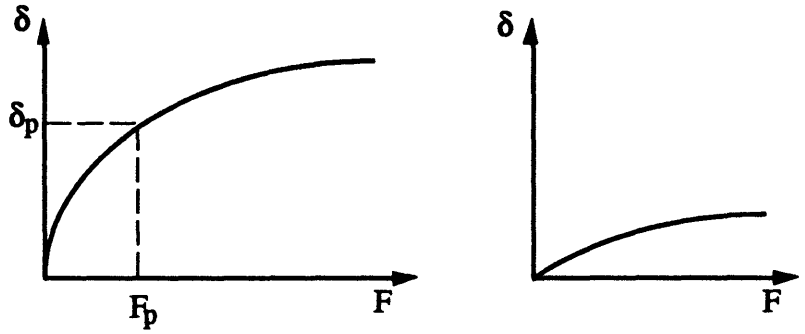

a) Non-preloaded Bearing Load-Deflection Curve. b) Preloaded Bearing Load-Deflection Curve.

Figure 1-5. Effects of Preload on Angular Contact Ball Bearing Deflection.

The graph on the left depicts a non-preloaded bearing's load deflection curve. If the bearing is set with a preload F_p, the resulting load deflection curve due to any applied load will appear as the graph on the right. Note that the curve on the right is the same as the portion of the left curve above F_p. By using preloaded bearings, the relative displacement is less and the stiffness is higher than for non-preloaded systems. The calculation procedure will be given in Sections 2 and 3 for the generation of load deflection curves for both angular contact ball bearings and tapered roller bearings.

2.0

Angular Contact Ball Bearing Characteristics.

To aid in the design effort of the tapered roller bearing, the angular contact ball bearing was evaluated in terms of the ballscrew application's critical parameters, axial stiffness and torque. These characteristics are derived and challenged experimentally in the following section for both the single and triplex angular contact ball bearings.

2.1 Axial Deflection and Stiffness Calculations.

To calculate the axial deflection and axial stiffness values for angular contact ball bearings, the normal deflections across the balls in the raceways will be solved. In doing so, the relative approach of remote points in the contacting bodies can be extended to represent the axial approach of the angular contact ball bearing rings[1]. This relative approach is equivalent to the axial deflection of the bearing. By constructing a curve of axial deflection versus axial load, the axial stiffness values can be determined by analyzing the slope of the line tangent to the load deflection curve at the point in question. For the following calculations, the assumption of rigid rings is used such that telescoping issues do not complicate the solution.

2.1.1 Single Row Angular Contact Ball Bearing.

The axial deflection calculation method outlined in this section delivers the load-deflection relationship seen in Figure 2-1. If the axial deflection of a pre-loaded system is desired under an applied load F_a, the relationship between the deflection δ_p, due to the preload F_p, and the resulting deflection δ_a, due to the applied axial load F_a, can be seen in Figure 2-1.

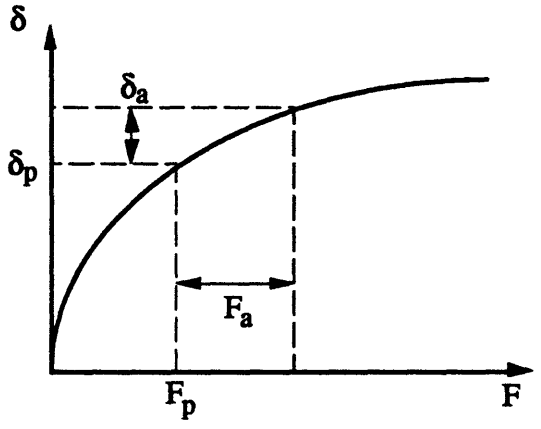

Figure 2-1. Axial deflection in a preloaded system.

[1] See also: T. A. Harris. Rolling Bearing Analysis. John Wiley & Sons, Inc. New York 1991

For preloaded systems, the externally applied loads F_a are in addition to any preloads already existing across the bearings. The following derivation of the axial deflection and resulting axial stiffness of a single angular contact ball bearing is for centric thrust loading only where the radial component of the applied load is much less than the thrust component.

$$F_a >> F_r \qquad F_r \approx 0$$

The above loading condition creates an environment in which the thrust load is shared equally amongst the balls in the raceway. To calculate the load on any one ball so that an evaluation of the Hertzian deformation between the ball and the inner and outer raceways can be performed, simple geometry leads us to the following relation:

$$Q_n = \frac{F_a}{Z \sin \alpha} \qquad 2.1$$

Q_n is the normal load on the ball, F_a is the axial load on the bearing, Z represents the number of balls in the raceway and α is the contact angle. The contact angle is defined as the line drawn through the points of contact that occur between the ball and the inner and outer raceways as shown in Figure 2-2.

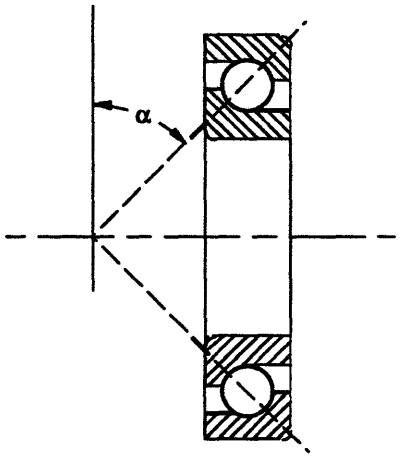

Figure 2-2. Illustration of the Contact Angle α.

It is important to note that as the angular contact ball bearing is loaded axially, the contact angle α, changes due to the deformations that take place between the raceways and the balls. Before solving for the resulting contact angle α due to an applied load F_a, the initial

unloaded contact angle α^o must be found. Be wary when using values of contact angles supplied by the bearing manufacturer. The values typically quoted are for the bearing when it is in the preloaded condition, or α prior to the influence of external loads. The most important thing to remember is that the contact angle changes when the load across the bearing changes. From strictly geometric considerations one can calculate the initial unloaded contact angle, α^o, for the ball bearing.

$$\alpha^o = \cos^{-1}\left(1 - \frac{P_d}{2BD}\right) \qquad 2.2$$

In the above equation D is the ball diameter, B is defined as the total curvature of the ball bearing which is a function of the groove radii and the ball diameter while P_d refers to the diametral clearance (free radial motion of the bearing in the mounted but unloaded condition).

$$B = \frac{r_i}{D} + \frac{r_o}{D} - 1 \qquad 2.3$$

$$P_d = d_o - d_i - 2D \qquad 2.4$$

In Equations 2.3 and 2.4 the basic dimensions of the ball bearing are introduced: inner groove radius r_i, outer groove radius r_o, inner raceway diameter d_i, and the outer raceway diameter d_o. From classical rolling bearing theory it has been shown that the normal deflection δ_n is related to the normal load across the rolling elements in the following fashion:

$$Q_n = K_n \delta_n^{1.5} \qquad 2.5$$

The exponent of the normal deflection δ_n is equal to 1.5 as we are assuming point contact between the ball and raceways. For line contact assumptions this exponent changes to 1.11. When a thrust load is applied to the bearing inducing an axial deflection δ_a, there is a normal component along the line of contact which can be defined as:

$$\delta_n = BD\left(\frac{\cos\alpha^o}{\cos\alpha} - 1\right) \qquad 2.6$$

Figure 2-3 illustrates the axial deflection and subsequent change in contact angle from α^o to α. In this illustration the bearing changes from an unloaded to a loaded condition.

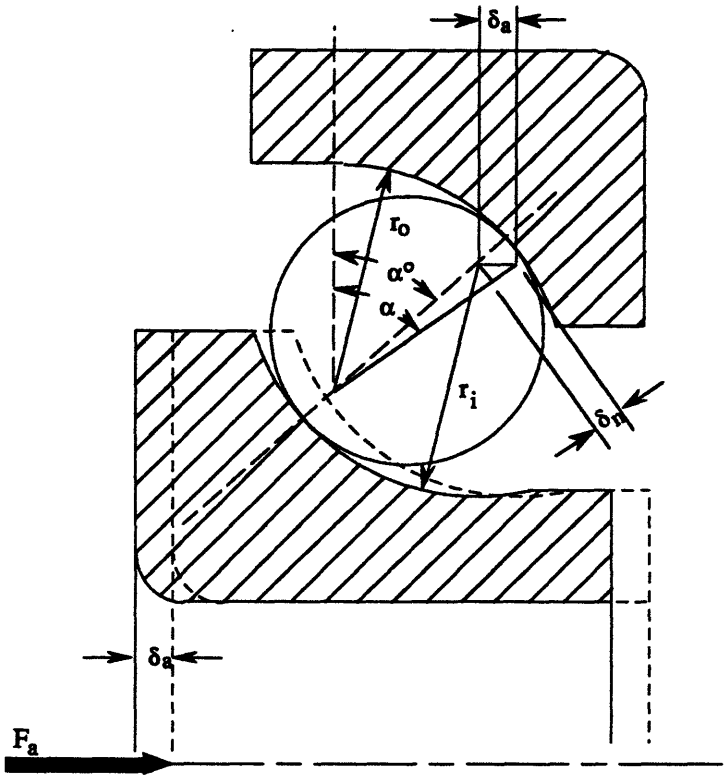

Figure 2-3. Change of Contact Angle under Thrust Load.

The quantity K_n defined in Equation 2.5 represents the load deflection factor and is also dependent upon the loaded contact angle α for computation. As both the load and deflection characteristics are dependent upon the contact angle α, an iterative approach must be used.

$$K_n = \left[\frac{1}{\left(\frac{1}{K_i}\right)^{\frac{1}{n}} + \left(\frac{1}{K_o}\right)^{\frac{1}{n}}}\right]^n \qquad 2.7$$

where $K_{i,o} = 3.12*10^7 \left(\Sigma\rho_{i,o}\right)^{-\frac{1}{2}} \left(\delta^*_{i,o}\right)^{-\frac{3}{2}}$ 2.8

for steel ball and raceway contact

To find the summations of the curvatures, $\Sigma\rho_{i,o}$ for the two conditions, ball/inner race and ball/outer race consider Figure 2-4:

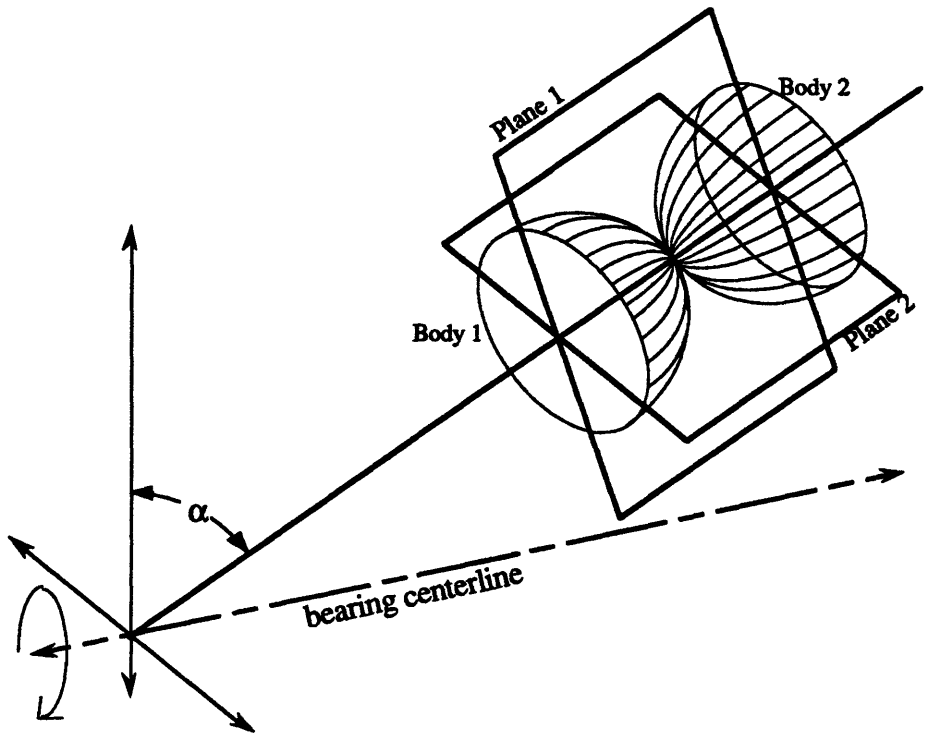

Figure 2-4. Geometry of Bodies Contacting Along Contact Angle.

To determine the curvature sum for the contacting bodies observe the two orthogonal planes seen in Figure 2-4. These planes intersect in a line oriented along the contact angle α passing through the point of contact of the two bodies. In these intersecting planes lie four radii defining the curvatures: $\rho_{11}, \rho_{12}, \rho_{21}$, and ρ_{22}. The curvature summation can be expressed as:

$$\Sigma\rho_{i,o} = \rho_{11} + \rho_{12} + \rho_{21} + \rho_{22} = \frac{1}{r_{11}} + \frac{1}{r_{12}} + \frac{1}{r_{21}} + \frac{1}{r_{22}} \qquad 2.9$$

Separating the above figure into the two intersecting planes to better illustrate the contacting geometry between the ball and the inner raceway we obtain the following cross sections which aid in defining the radii comprising the curvature summations:

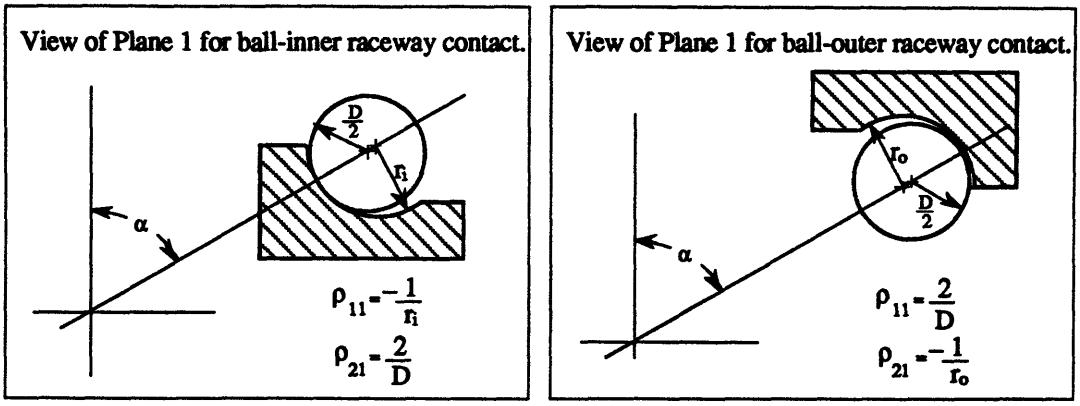

Figure 2-5. Planar Geometry for Ball-Inner Raceway Contact.

In the above figures the inner raceway is represented as body 1 while the ball is represented as body 2. Therefore ρ_{12} designates the curvature of body 1 in plane 2. The curvatures for the calculation of the inner curvature summation $\Sigma\rho_i$ through Equation 2.9 have been given in Figure 2-5. The quantity d_m represents the pitch diameter of the bearing.

$$d_m = \left(\frac{d_o + d_i}{2}\right) \qquad 2.10$$

Note the negative sign for ρ_{11}. It is imperative that all convex surfaces are positive while all concave surfaces are negative.

For the contact of the outer raceway and the ball, the ball was designated as body 1 while the outer raceway was designated as body 2. The cut planes can be seen below in Figure 2-6.

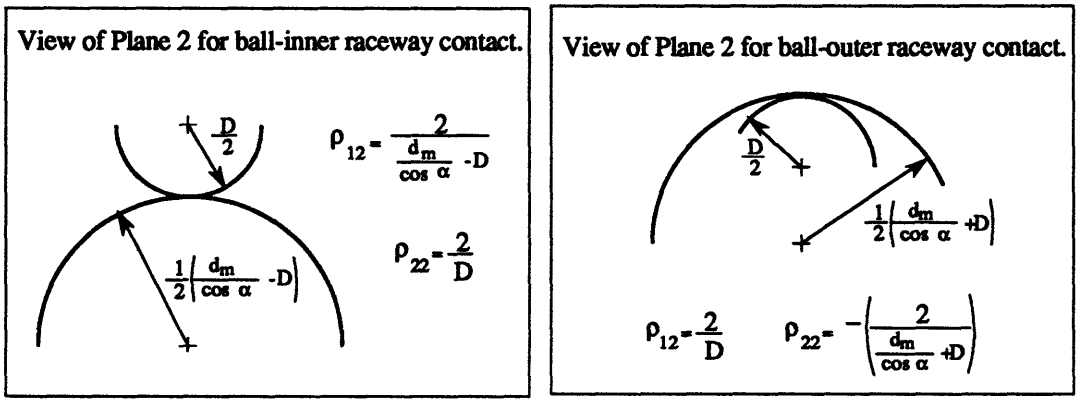

Figure 2-6. Planar Geometry for Ball-Outer Raceway Contact.

After determination of the curvatures for the ball-outer raceway contact, the outer curvature summation, $\Sigma\rho_o$, can be calculated using Equation 2.9. Once again, check to be sure that convex surfaces have positive curvatures while concave surfaces have negative curvatures. Combining Equations 2.8 and 2.9 with the values from Figures 2-5 and 2-6 allows K_n to be rewritten as:

$$K_n = \left[\frac{1}{\left(\frac{1}{3.12*10^7 \left(\frac{-1}{r_i} + \frac{2}{\frac{d_m}{\cos\alpha} - D} + \frac{2}{D} + \frac{2}{D} \right)^{-\frac{1}{2}} \left(\delta^*_i\right)^{-\frac{3}{2}}} \right)^{\frac{1}{n}} + \left(\frac{1}{3.12*10^7 \left(\frac{2}{D} + \frac{2}{D} + \frac{-1}{r_o} + \frac{-2}{\frac{d_m}{\cos\alpha} + D} \right)^{-\frac{1}{2}} \left(\delta^*_o\right)^{-\frac{3}{2}}} \right)^{\frac{1}{n}} } \right]^n$$

Again $n = 1.5$ for point contact. The final parameter to be quantified is the dimensionless contact parameter δ^*. Once this value is determined, K_n can be solved leading to the determination of the axial deflection and stiffness.

The value of δ^* is the dimensionless parameter dealing with the relative approach of two curved bodies and is related to the deformation that takes place between them. In the deformation of the curved surfaces seen in Figure 2-4 two things happen. First remote points within the two bodies approach each other by the amount δ. Secondly, an elliptical contact area is formed between the two curved bodies defined by the dimensions of the semimajor and semiminor axes a and b. Figure 2-7 Illustrates these concepts.

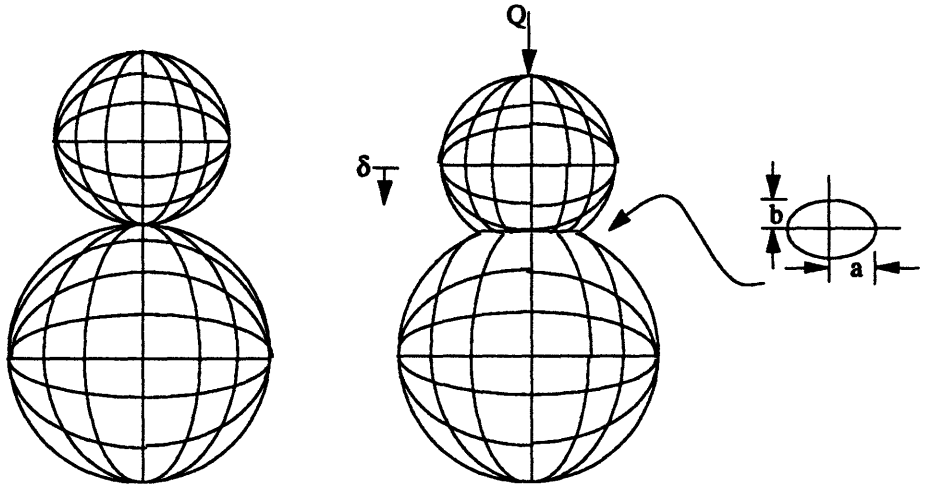

Figure 2-7. Illustration of Contact Parameters δ, a, and b.

In short, the contact area defined by the ellipse with axes $2a$ and $2b$ results from the relative approach δ which is governed by the load and geometry of the bodies. These three quantities δ, a, and b describing the physical characteristics of the contact deformation can be expressed as:

$$a = \left(\frac{2k^2\mathfrak{E}}{\pi}\right)^{\frac{1}{3}}\left[\frac{3Q}{2\Sigma\rho}\left(\frac{(1-\xi_1)^2}{E_1}+\frac{(1-\xi_2)^2}{E_2}\right)\right]^{\frac{1}{3}} \qquad 2.11$$

$$b = \left(\frac{2\mathfrak{E}}{\pi k}\right)^{\frac{1}{3}}\left[\frac{3Q}{2\Sigma\rho}\left(\frac{(1-\xi_1)^2}{E_1}+\frac{(1-\xi_2)^2}{E_2}\right)\right]^{\frac{1}{3}} \qquad 2.12$$

$$\delta = \frac{2\mathfrak{F}}{\pi}\left(\frac{\pi}{2k^2\mathfrak{E}}\right)^{\frac{1}{3}}\left[\frac{3Q}{2\Sigma\rho}\left(\frac{(1-\xi_1)^2}{E_1}+\frac{(1-\xi_2)^2}{E_2}\right)\right]^{\frac{1}{3}}\left(\frac{\Sigma\rho}{2}\right) \qquad 2.13$$

In the above Equations, $E_{1,2}$ represents the Young's modulus for the materials of bodies 1 and 2 while $\xi_{1,2}$ represent the Poisson's ratios. Also, k=a/b and the variables $\mathfrak{F}$ and $\mathfrak{E}$ are the complete elliptic integrals of the first and second kind:

$$\mathfrak{F} = \int_0^{\frac{\pi}{2}}\left[1-\left(1-\frac{1}{k^2}\right)\sin^2\phi\right]^{\frac{-1}{2}}d\phi \qquad 2.14$$

$$\mathfrak{E} = \int_0^{\frac{\pi}{2}}\left[1-\left(1-\frac{1}{k^2}\right)\sin^2\phi\right]^{\frac{1}{2}}d\phi \qquad 2.15$$

Unfortunately, there is no direct integration to solve for the above integrals[1]. Equations 2.14 and 2.15 evaluate the first quadrant of the elliptical contact area's footprint. These integrals can be solved through numerical integration using Simpson's Rule to generate the values of δ, a, and b in Equations 2.11, 2.12, and 2.13.

---

[1] See also: A. H. Slocum. Precision Machine Design. Prentice Hall, New Jersey. 1992 pg. 228-235

Conveniently, there is a relationship between a property known as the curvature difference $F(p)$ and the elliptic integrals of the first and second kind.

$$F(p)_{i,o} = \frac{[(\rho_{11} - \rho_{12}) + (\rho_{21} - \rho_{22})]_{i,o}}{\Sigma\rho_{i,o}} \qquad 2.16$$

$$F(p)_{i,o} = \frac{(k^2 + 1)\mathfrak{E} - 2\mathfrak{F}}{(k^2 - 1)\mathfrak{E}} \qquad 2.17$$

The curvature difference in Equation 2.16 can be solved directly from the geometry of the two contacting bodies as was detailed through Equation 2.9 and the equations in Figures 2-5 and 2-6. $F(p)$ is a dimensionless value and the dimensionless values of δ, a, and b, namely δ^*, a^*, and b^* can be expressed as functions of $F(p)$. Table 2-1 summarizes the relationships between the dimensionless parameters $F(p)$, δ^*, a^*, and b^*.

Table 2-1. Relationship of $F(p)$ to the dimensionless contact parameters δ^*, a^*, and b^*.

F(p)	δ^*	a^*	b^*
0	1	1	1
0.1075	0.9974	1.0760	0.9318
0.3204	0.9761	1.2623	0.8114
0.4795	0.9429	1.4556	0.7278
0.5916	0.9077	1.6440	0.6687
0.6716	0.8733	1.8258	0.6245
0.7332	0.8394	2.011	0.5881
0.7948	0.7961	2.265	0.5480
0.83495	0.7602	2.494	0.5186
0.87366	0.7169	2.800	0.4863
0.90999	0.6636	3.233	0.4499
0.93657	0.6112	3.738	0.4166
0.95738	0.5551	4.395	0.3830
0.97290	0.4960	5.267	0.3490
0.983797	0.4352	6.448	0.3150
0.990902	0.3745	8.062	0.2814
0.995112	0.3176	10.222	0.2497
0.997300	0.2705	12.789	0.2232
0.9981847	0.2427	14.839	0.2072
0.9989156	0.2106	17.974	0.18822
0.9994785	0.17167	23.55	0.16442
0.9998527	0.11995	37.38	0.135050
1	0	infinite	0

Dimensionless values for δ, a, and b have been presented to allow the universal applications of this calculation method, and quick reference to the value of δ^* for the computation of K_n.

The relationship between $F(p)$ and δ^* can be seen graphically in Figure 2-8.

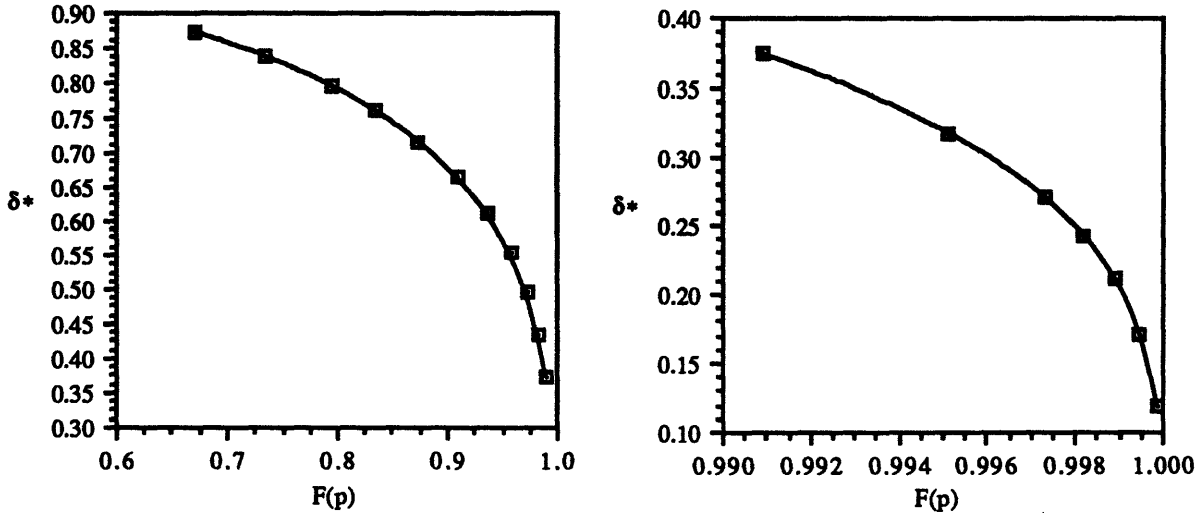

Figure 2-8. Relationship Between $F(p)$ and δ^*.

A curve fit was applied to Figure 2-8 so that the relationship between F(p) and d* could be used in a spreadsheet. The following equation details the above graphical relationship:

$$\delta^* = .13013 + 12.787\left\{[-(\log F(p))]^{.667}\right\} - 148.46\left\{[-(\log F(p))]^{.667}\right\}^2 + 956.25\left\{[-(\log F(p))]^{.667}\right\}^3 - 2925.8\left\{[-(\log F(p))]^{.667}\right\}^4 + 3346.3\left\{[-(\log F(p))]^{.667}\right\}^5 \qquad 2.18$$

The dimensionless quantities of Table 2-1 are related to the elliptic integrals of the first and second kind by the following relations:

$$a^* = \left(\frac{2k^2\mathbf{E}}{\pi}\right)^{\frac{1}{3}} \qquad 2.19$$

$$b^* = \left(\frac{2\mathbf{E}}{\pi k}\right)^{\frac{1}{3}} \qquad 2.20$$

$$\delta^* = \frac{2\mathcal{F}}{\pi}\left(\frac{\pi}{2k^2\mathcal{E}}\right)^{\frac{1}{3}} \qquad 2.21$$

Refer back to Equations 2.11, 2.12, and 2.13 to see the established relationships come full circle: $F(p)$ to δ^*, a^*,b^*, to δ, a, b, to $\mathcal{E}$,$\mathcal{F}$ and back to $F(p)$. In more detail, $F(p)$ is defined by the geometry of the bodies in contact. The value of $F(p)$ can be matched to values of δ^*, a^*, and b^* through Table 2-1 summarizing the curvature dependent deformation parameters. The values of δ^*, a^*, and b^* are next transformed from dimensionless quantities into δ, a, and b through the load, geometry, and material considerations of Equations 2.11, 2.12, 2.13. Substitution of $k=a/b$ into equations 2.14 and 2.15 allows the calculation of the elliptic integrals which in turn describe $F(p)$.

Returning to the calculation for the axial deflection and axial stiffness of the angular contact ball bearing, solving for $F(p)$ and referring to the above table, graph, or approximation for the corresponding value of δ^*, K_n can be calculated based upon the contact angle α. Combining Equations 2.1, 2.5, and 2.6 creates the equality that must be established through the iteration of the contact angle α.

$$\frac{F_a}{Z \sin\alpha} = K_n\left[B\,D\left(\frac{\cos\alpha^o}{\cos\alpha} - 1\right)\right]^{1.5} \qquad 2.22$$

Once a value of α has been found which satisfies Equation 2.22, the axial deflection and axial stiffness of the thrust loaded angular contact ball bearing can be calculated.

$$\delta_a = \frac{B\,D\sin(\alpha - \alpha^o)}{\cos\alpha} \qquad 2.23$$

The axial stiffness is defined as the inverse of the slope of the line tangent to the load-deflection curve generated using the preceding equations.

Creating a numerical iteration scheme to balance Equation 2.22 using values of the contact angle , α, one can develop an active axial deflection and axial stiffness calculator for an angular contact ball bearing. A schematic diagram shows the interrelationships between the bearing parameters and the eventual computation path used for the calculations. Parameters that must be entered into the system are found in the rounded cells. The remaining cells represent calculations.

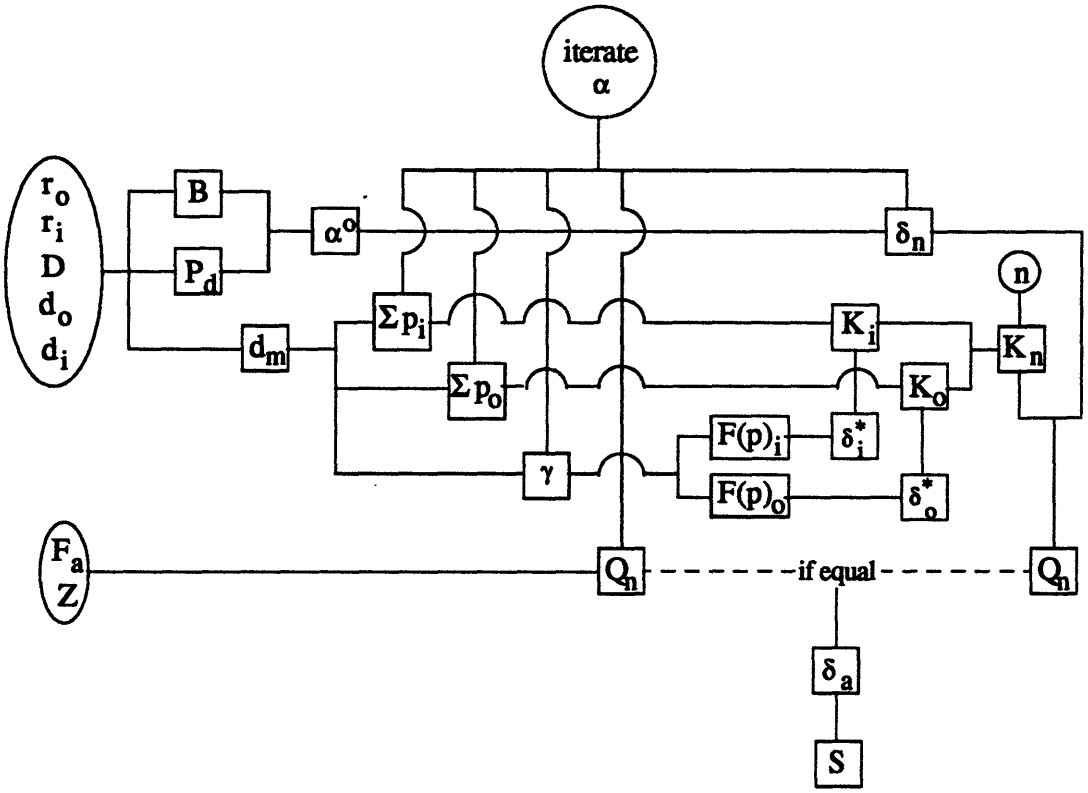

Figure 2-9. Angular Contact Ball Bearing Calculation Flowchart.

A sample spreadsheet has been created to perform the deflection and stiffness calculations for an angular contact ball bearing using Equations 2.1 through 2.23 and the calculation flow path seen in Figure 2-9.

The following spreadsheet calls for the iteration of the contact angle α to obtain values for the axial deflection at the desired load. The iteration is complete when the iteration balance reads zero. Referring to the spreadsheet, with the specified bearing parameters an axial deflection of 0.000732" can be expected under a thrust load of 2040 lbs. Using the spreadsheet, a load-deflection curve can be generated from which the slope of the curve at any point will give the axial stiffness of the bearing under those conditions. For the conditions in Figure 2-10, the angular contact ball bearing has a theoretical axial stiffness of 4.0×10^6 lb/in under an axial load of 2040 lbs.

Angular Contact Ball Bearing Axial Deflection Calculator

Bearing Parameters	(lb,in,°)	(N,mm,rad)
Z	18.	
D	0.343750	8.731250
d_i	1.817159	46.155839
d_o	2.520305	64.015747
r_i	0.178750	4.540250
r_o	0.182188	4.627563
d_m	2.168732	55.085793
Q_n	133.249290	592.69284
B	0.050000	0.050000
P_d	0.015646	0.397408
α^o	56.986021	0.994594
$\Sigma\rho_i$	0.2587032	
$\Sigma\rho_o$	0.2244028	
$F(p)_i$	0.9318904	
$F(p)_o$	0.9013479	
δ^*_i	0.617678	
δ^*_o	0.667269	
K_i	870751.2263	
K_o	832669.2009	
K_n	300958.5107	

Axial Load (lb)	(N)
2040.00	9073.92

Contact Angle (°)	(rad)
58.270028	1.017003

iteration balance
0.000000

Axial Deflection (in) = 0.000732

inner/outer contact area = 0.0065 in^2

Figure 2-10. Angular Contact Ball Bearing Spreadsheet.

A good first order approximation of angular contact ball bearing axial deflection has been presented in Harris' Rolling Bearing Analysis[1]. This approximation allows quick back-of-the-envelope estimations of axial deflection which can be used to create a load deflection curve to determine rough stiffness values.

$$\delta_a = 1.58 \times 10^{-5} \frac{Q^{.667}}{D^{.333} \sin \alpha} \qquad 2.24$$

In this equation, $Q = F_a/(Z \sin\alpha)$ with the axial load, F_a, in lbs and the ball diameter, D, in inches.

Analysis of the contact areas that are formed between the balls and the raceways is useful in assessing bearing heat generation. Working from the geometric relationship of $F(p)$ established in Equation 2.16, values of a^* and b^* can be gathered from Table 2-2 and used

[1] T. A. Harris. Rolling Bearing Analysis. John Wiley & Sons, Inc. New York 1991 pg. 328.

with Equations 2.11 and 2.12 to calculate the inner and outer contact areas. This has been done for the MM35BS72 angular contact ball bearing and can be seen in the following graphs relating the elliptical contact areas to the axial load and axial deflection.

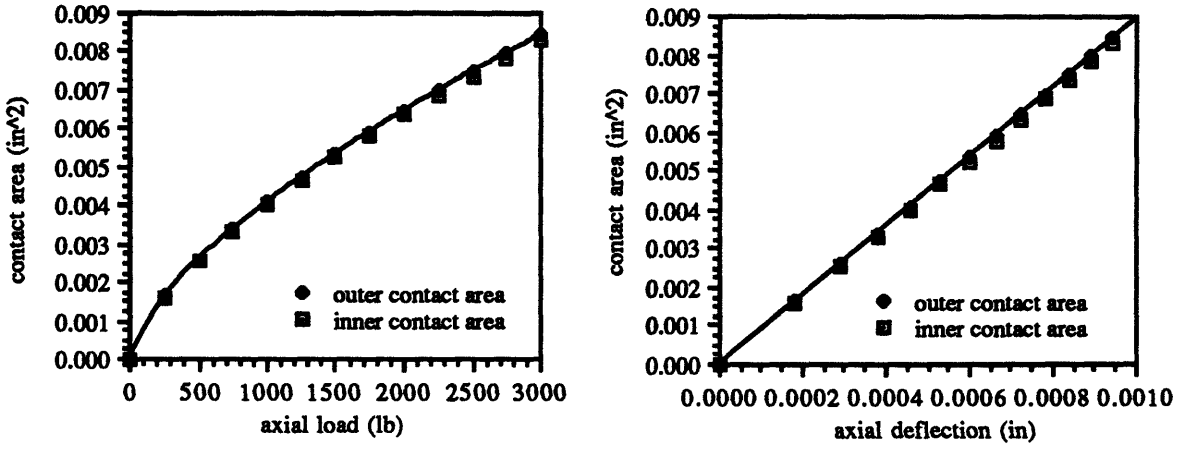

Figure 2-11. Elliptical Contact Area as a Function of Load and Deflection.

The calculation procedure for the contact area that forms between the balls and the raceways is similar in fashion to the calculation of δ^*. Once $F(p)$ is calculated through the geometric relationship of Equation 2.16, the values in Table 2-1 are used to determine the dimensionless contact parameters a^* and b^*. Knowing these values, they can be substituted into Equations 2.11 and 2.12 to solve for the semimajor and semiminor axes of the elliptical contact area. Curve fitting the values of $F(p)$ to the values of a^* and b^* delivers the following relationships that can be used in spreadsheets to calculate the values of a and b for varying load conditions.

$$\frac{1}{\log a^*} = .71288 + 14.701\left\{\left[-(\log F(p))\right]^{.667}\right\} - 49.315\left\{\left[-(\log F(p))\right]^{.667}\right\}^2 + 158.98\left\{\left[-(\log F(p))\right]^{.667}\right\}^3 - 190.41\left\{\left[-(\log F(p))\right]^{.667}\right\}^4 + 99.340\left\{\left[-(\log F(p))\right]^{.667}\right\}^5 \qquad 2.25$$

$$\frac{1}{-\log b^*} = 1.0689 + 55.224\left\{\left[-(\log F(p))\right]^{.667}\right\} - 366.71\left\{\left[-(\log F(p))\right]^{.667}\right\}^2 + 2007.3\left\{\left[-(\log F(p))\right]^{.667}\right\}^3 - 3894.5\left\{\left[-(\log F(p))\right]^{.667}\right\}^4 + 3192.6\left\{\left[-(\log F(p))\right]^{.667}\right\}^5 \qquad 2.26$$

Using the above relationships between $F(p)$ and the dimensionless contact parameters a^* and b^* along with Equations 2.11 and 2.12, the elliptical contact area can be found as:

$$A_{\text{elliptical contact}} = \pi (ab) \qquad 2.27$$

2.1.2 Triplex Angular Contact Ball Bearing.

The results obtained through Section 2.1.1 for the single angular contact ball bearing can be extended to calculate the axial deflection and axial stiffness of any mounting condition. Consider the stackup of three angular contact ball bearings in a triplex arrangement as in Figure 2-12.

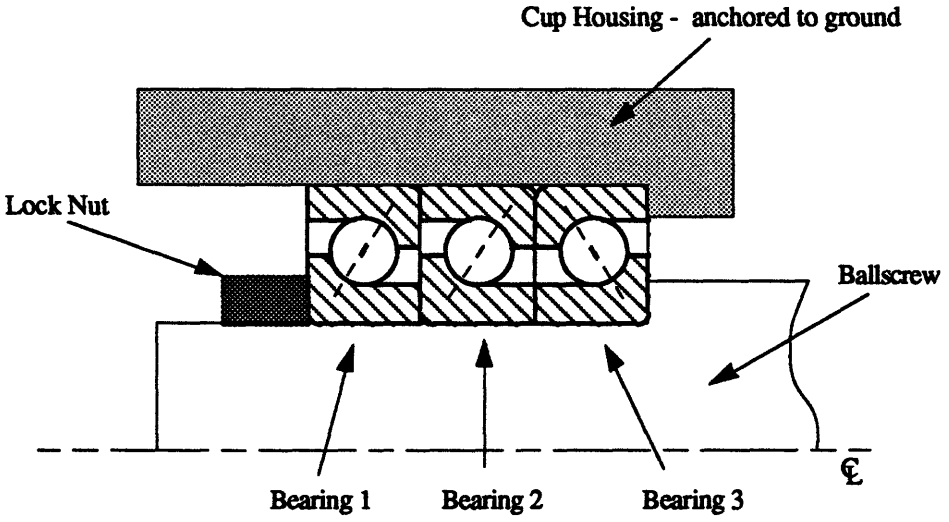

Figure 2-12. Triplex Angular Contact Ball Bearing System.

Multiple rows of bearings are used to increase the load carrying capability and alter shaft end-conditions in applications. When multiple rows of bearings are used to support a shaft subjected to tilting moments about the bearings, the shaft-ends can be modelled as if they are sunk into a wall. This improves the stiffness of the shaft system as the deflection and rotational characteristics are improved.

By calculating the forces that exist across each of the angular contact ball bearings, stiffness values can be generated for the individual bearings which can be summed in parallel to represent a composite bearing package stiffness. A parallel summation of the stiffnesses is used due to the perfect load sharing assumption that will be detailed later. To calculate the

loading conditions that exist across a ball bearing stack-up, start with the preload conditions.

When the bearings are tightened against the shoulder of the ballscrew using the locknut, the preload force is established within the bearing system. The value of the preload within the bearing is set by the manufacturer as discussed in the introduction to Section 2.0. Knowing the amount of the load that is 'within' the bearings when they are tightened down such that their raceways are in contact with each other is imperative. Without this information it is very difficult to calculate the resulting effects of externally applied loads to the bearing system and their effects on the deflections and stiffnesses. A single MM35BS72 angular contact ballscrew support bearing is manufactured with a preload of 1500 lbs. This can be verified by looking at the single bearing load-deflection curve. When the curve is obtained experimentally as in Section 2.2, it can be inversed about the load axis and the point of intersection determines the amount of preload within the elastic region of deformation of the bearing. Figure 2-13 illustrates the graphical method of verifying bearing preload.

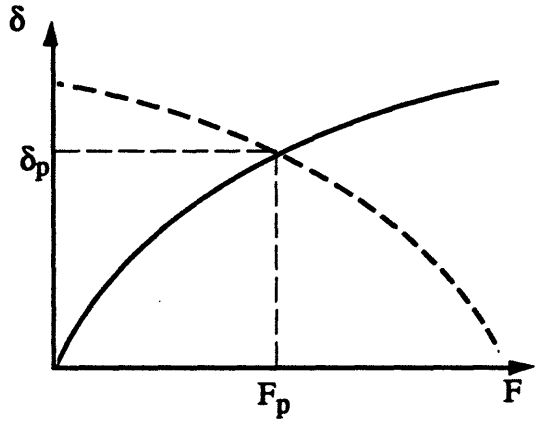

Figure 2-13. Determination of Bearing Preload from the Load-Deflection Curve.

At the intersection of the load deflection curve and its inverse, the resulting axial load is 1500 lbs and the axial deflection is 0.000598". This means that it takes 1500 lbs of axial load to close the gap that is ground in by the bearing manufacturer. When stacking up three angular contact ball bearings in triplex fashion as in Figure 2-12, the amount of preload that will exist in the system is different than the amount of preload that exists across a single bearing. This is because the preload force stems from the closing of the gaps that are

ground into the bearings by the manufacturer. The total gap within the triplex system is twice that for the single bearing. Figure 2-14 illustrates the gap locations in the triplex system before they are squeezed shut during preloading.

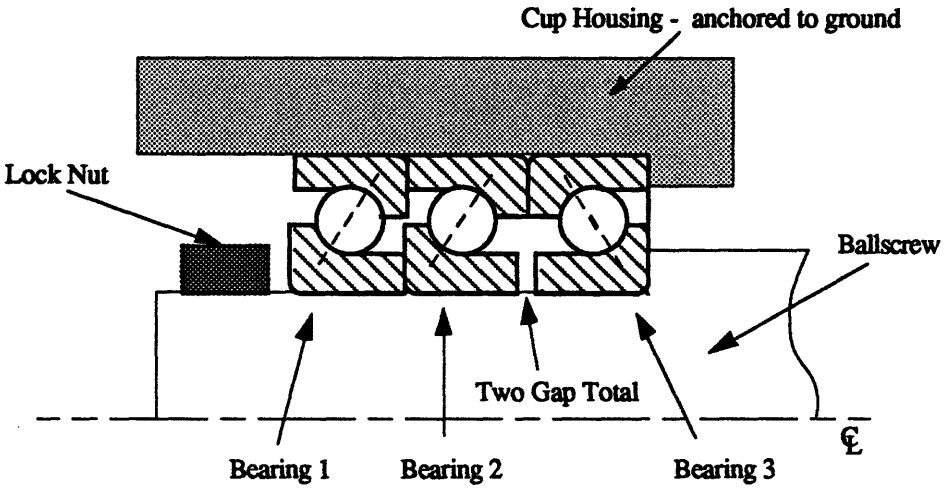

Figure 2-14. Illustration of Gap Locations in Non-Preloaded Triplex Stack-up.

Notice that there is no gap between the two tandem bearings. This is because the inner and outer raceways are ground to the same width. With the introduction of the balls, the raceways are 'spread'. Looking at Bearing 1 of Figure 2-14, the inner race extends out to the left while the outer race extends the same amount to the right. Figure 2-14 also illustrates how similar bearings oriented in the same direction do not expose a gap as the amount of 'extension' of the raceways on either side of the ball are equal. However, when placing bearings in opposing directions such as Bearings 2 and 3 of Figure 2-14, the two gaps are exposed. Therefore, the total gap to be closed for the triplex arrangement of the MM35BS72 angular contact ball bearings is twice the single bearing gap and is equal to 0.001196".

Under the perfect load sharing assumption, the two tandem bearings each carry the same amount of axial load, the sum of which is equal to the load carried by the third bearing, oriented in the opposing direction. In order to find the amount of load across each of the bearings in the triplex system when the gaps are closed, or preloaded, we return to the load-deflection curve for the single bearing. The following conditions must be satisfied: the load across each of the tandem bearings must be half that across the third opposing

bearing, and the sum of the axial deflections of the tandem pair and the third opposing bearing must equal twice the axial deflection of the single bearing under preload.

For the triplex stack-up of MM35BS72 angular contact ball bearings, the load across Bearings 1 and 2 is 1020 lbs while Bearing 3 opposes them with 2040 lbs. At 1020 lbs, the axial deflection is 0.000464" and at 2040 lbs the axial deflection is 0.000732" amounting to a sum of 0.001196", equal to twice the single bearing gap. For the triplex arrangement, the amount of preload can also be found through the following relationship:

$$F_p' = 1.36\, F_p \qquad 2.28$$

F_p' represents the triplex preload force while F_p represents the preload ground into a single bearing. To calculate the stiffness of the triplex system in the preloaded condition it is necessary to compute the individual bearing stiffnesses under their individual loads and then sum the stiffnesses.

$$S_{\text{triplex under preload}} = S_{1020} + S_{1020} + S_{2040} \qquad 2.29$$

The stiffnesses are summed as if they were springs operating in parallel because of the perfect load sharing assumption. Figure 2-15 illustrates the perfect load-sharing assumption for the triplex system.

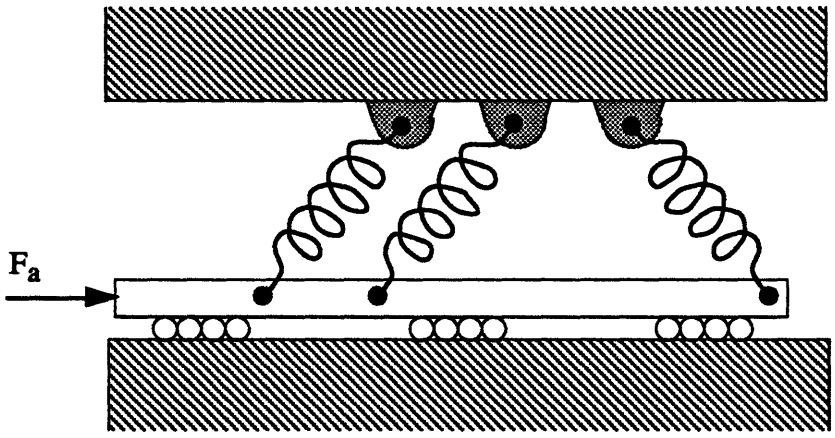

Figure 2-15. Parallel Spring Model of Perfect Load Sharing Assumption.

The individual stiffnesses S_{1020} (axial stiffness at 1020 lbs) and S_{2040} can be found by looking at the slope of the load-deflection curve for the single bearing.

Knowing the load across the preloaded bearings is critical in predicting the results of external forces to the system. One such externally applied load that will be discussed further in Section 4.1 is the stretch that is applied to a ballscrew shaft to improve various operating characteristics. If a stretch is induced resulting in an additional 2000 lbs of axial force that must be carried by the support bearings, each of the triplex ends on the ballscrew would have to assume 1000 lbs of the stretch load. This load, since it is trying to pull the bearings towards the center of the ballscrew, would create the following load conditions within the triplex system: Bearings 1 and 2 would carry 1520 lbs axially while Bearing 3 would be loaded with 1040 pounds. Remember that the 1000 lbs is in addition to the preload within the bearing system. Referring to Figure 2-15 and assuming that the stretch load is equal to F_a, it can be seen how the two bearings in tandem will go into a state of compression (addition of load) while the third bearing will move in a tensile fashion (subtraction of load). Remember that the perfect load sharing model assumes that the three inner rings are contacting and that they will all move along the axis together when subjected to an applied axial load. The resulting stiffness value of the triplex system can be re-evaluated under the new loading conditions:

$$S_{\text{triplex under preload and stretch}} = S_{1520} + S_{1520} + S_{1040} \qquad 2.30$$

This procedure holds for any loading condition and any mounting arrangement.

Triplex system stiffnesses will be detailed for the ballscrew application in Section 4.0 relating to ballscrew stretch conditions, thermal concerns, and externally applied loads.

2.2 Angular Contact Ball Bearing Axial Deflection Experiment.

In an attempt to verify the theory presented in Section 2.1, a series of non-rotating deflection tests were run with the angular contact ball bearings. Axial deflection measurements were made on a single angular contact ball bearing and a load-deflection curve generated similar to that seen in Figure 2-1. From the experimental curve generated in Figure 2-17, the stiffness values of the single angular contact ball bearing can be taken as the inverse of the slope at the load in question. Figure 2-16 shows the set-up for the axial deflection test.

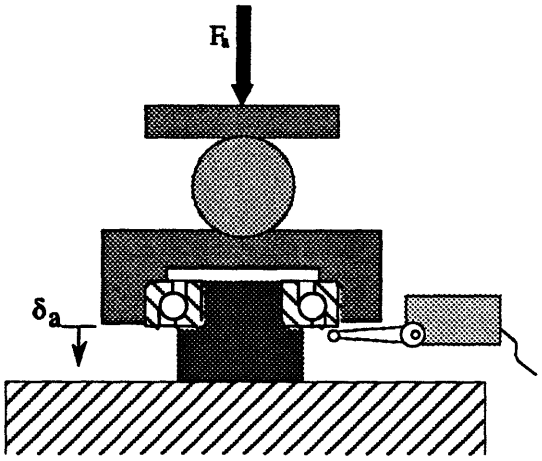

Figure 2-16. Angular Contact Ball Bearing Axial Deflection Test Set-up.

A Baldwin Universal Tester was used to administer the axial load to the bearing. The load was distributed by way of a steel sphere set within two piloted mounts. The outside and inside diameters were constrained such that telescoping effects would not influence the axial deflection results. Telescoping can be thought of as a radial expansion or contraction of the bearing raceways under load. The toleranced fits for constraining the inside and outside diameters of the bearings were taken from the specifications for the required fits of the ballscrew system.

Shaft and Shoulder Tolerances for MM35BS72 Angular Contact Ball Bearing

shaft diameter	34.995mm - 34.990mm
housing diameter	72.008mm - 72.000mm
shaft shoulder diameter	42.0mm ±0.13mm
housing shoulder diameter	64.0mm ±0.13mm
max fillet radii	0.80mm

Measurements of the axial deflection were made using ball tipped contact styluses at three points spaced 120° apart. The styluses touched off along the ground bottom face of the bearing outer raceway as seen in Figure 2-16. The three values were averaged to generate a more accurate value for the axial deflection. After the deflection test was run, the bearing was removed and the deflection within the fixturing elements was evaluated. The curve resulting from the mechanical deflection of the fixture was subtracted from the load-deflection curve obtained with the bearing. The resulting curve is the true deflection of the bearing minus any fixturing effects and can be seen in Figure 2-17 along with the theoretical curve generated in Section 2.1.

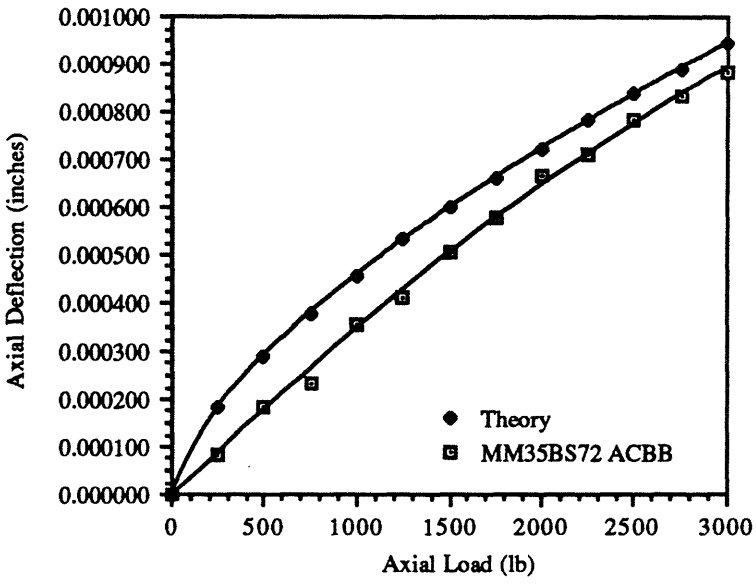

Figure 2-17. Comparison of Experimental and Theoretical Results for MM35BS72 Angular Contact Ball Bearing Axial Deflection.

From Figure 2-17 the axial stiffnesses at any point along the curves can be found by taking the inverse slopes at the load in question. Table 2-2 summarizes the experimental and theoretical static stiffnesses for the MM35BS72 angular contact ball bearing.

Table 2-2. Static Stiffnesses for MM35BS72 Angular Contact Ball Bearing

axial load (lb)	single bearing stiffness (lb/in)	theoretical stiffness (lb/in)
250	2.730e+6	1.889e+6
500	2.833e+6	2.421e+6
750	2.944e+6	2.781e+6
1000	3.063e+6	3.066e+6
1250	3.193e+6	3.307e+6
1500	3.335e+6	3.524e+6
1750	3.489e+6	3.725e+6
2000	3.659e+6	3.914e+6
2250	3.846e+6	4.087e+6
2500	4.053e+6	4.248e+6
2750	4.284e+6	4.393e+6
3000	4.542e+6	4.519e+6

Notice how the axial stiffness increases with increasing axial load. This is due to the changing contact angle which allows for better load transfer between the raceways. From

the above table it is clear that operation under preloaded conditions are definitely desirable to maintain elevated stiffness values.

The theory appears to be a fair approximation of the experimental system. Careful attention to the approximation procedure of evaluating the elliptic integrals can close the difference between the theoretical and experimental values. The theoretical stiffnesses calculated are within roughly 10% of the experimental values.

2.3 Angular Contact Ball Bearing Torque Calculations.

Bearings in rolling contact are often referred to as anti-friction bearings. Although the frictional values of these bearings are subsequently smaller than for bearings in sliding contact, the rolling bearing is not devoid of all friction, hence the term anti-friction is somewhat of a misnomer. The friction within a bearing can be thought of as a retarding torque or a resistance to motion. This internal friction generates heat and vibration causing thermal growth and accelerated bearing wear. It is desirable to keep bearings cool while running as they are often responsible for system alignment, load carrying capacity, and safe machine operation. The main sources of bearing friction stem from the following areas:

- material elastic hysteresis while rolling
- microslip of the rolling element along the raceway due to bearing geometry
- microsliding induced by deformation of the contacting bodies
- microslip between the rolling elements and the cage
- viscous drag of the lubricant on the revolving elements
- seal friction

The above areas are all contributors to the total friction present within the rolling bearing. Of these areas the most significant in reference to the angular contact ball bearing are the frictional effects due to the running resistance and the friction due to the sliding and hysteresis effects while rolling.

Palmgren set forth an empirical relation for the calculation of the torque of an angular contact ball bearing based upon several controlled studies. It was found that the bearing torque M could be expressed as the summation of the torque components due to the running resistance M_0 and the sliding and hysteresis resistance M_1. These components are

calculated as being independent of dynamic loads. In ballscrew applications, the effects of dynamic loads are small when compared to the static loads of bearing preload and ballscrew stretch. To calculate the torque due to the running resistance Palmgren[1] developed the relationship:

$$M_o = 8.66e^{-2}\, f_o\, p\, d_m^3 \left(\frac{\eta\, \omega}{p}\right)^{\frac{3}{2}} \qquad 2.31$$

The constant in front of the equation is used to change the units from kg-mm to lb-in. The other variable in Equation 2.31 represent the following: f_o is the bearing design and lubrication factor, p is the difference between atmospheric pressure and the vaporization pressure of the oil in kg/mm^2, d_m is the pitch diameter in mm, η is the dynamic viscosity of the lubricant in units of kg-sec/mm^2, and ω is the angular velocity of the bearing rings in relation to each other in rad/s.

Normally p is negligible so p = *atmospheric pressure*. An important assumption in the above equation is that the film thickness does not drop below one micron (40 microinches). Should this happen, due to surface roughnesses on the rolling elements and the raceways, the hydrodynamic theory no longer applies. To maintain this assumption the following must be true: $\eta\omega/p \geq 2e^{-6}$. The bearing design and lubrication factor f_o is related to the number of angular contact ball bearings by $f_o=2b$ where b is the number of bearings under consideration. In bearings using grease, η and p refer to the base oil used and the above values for f_o only hold for grease lubricated bearings shortly after they have been lubricated due to thermally induced lubricant viscosity breakdown which is difficult to accurately quantize.

If $vn \geq 2000$ Equation 2.31 can be modified into a more useable form

$$M_o = 8.66e^{-10}\, f_o\, d_m^3\, (v\, n)^{0.667} \qquad 2.32$$

where v is the kinematic viscosity in cSt (mm^2/sec) and n is the rotational speed in rpm. Using Equations 2.10 and 2.32 with values of $27cSt$ for the kinematic viscosity, v, of the Kluber Topas Isoflex NB52 grease specified for the ballscrew system, a shaft speed of

---

[1] A. Palmgren. Ball and Roller Bearing Engineering. 3rd ed., Burbank, Philadelphia (1959)

1450rpm necessary to achieve a rapid traverse speed of 800 ipm with the ballscrew lead, and f_o equal to 2, M_o= *0.33* in-lb for the MM35BS72 angular contact ball bearing.

To calculate the amount of sliding and hysteresis resistance M_1 in the bearing, Palmgren offers the following empirical relation:

$$M_1 = 8.66e^{-2}\, f_1\, g_1 d_m\, P_o \qquad 2.33$$

Again, the constant $8.66e^{-2}$ alters the units of M_1 from kg-mm to lb-in. f_1 is the bearing design and load factor, g_1 is a constant based on load orientation, P_o is the static equivalent load in kg factor and d_m is the pitch diameter in mm.

Palmgren found that for an angular contact ball bearing having a contact angle, α, of approximately 60°,

$$f_1 \approx 0.0013 \left(\frac{P_o}{C_o}\right)^{\frac{1}{3}} \qquad 2.34$$

The static equivalent load factor P_o can be expressed as

$$P_o = X_o F_r + Y_o F_a \qquad 2.35$$

where X_o is equal to 0.5 for the angular contact ball bearing, F_r is the radial component of the maximum static load in kg, and F_a is the axial component of the maximum static load in kg. The quantity Y_o is dependent upon the depth of the raceway groove and the bearing diametral clearance. A value of 0.3 for Y_o is acceptable as long as the contact load zone does not override the raceway causing load zone truncation and excessive raceway loading. This can be determined from geometric considerations based upon the contact angle α and the elliptic load zone diameters a and b.

The basic static load rating C_o is related to the load on the maximum loaded rolling element such that

$$C_o = Q_{max}\, i\, z \sin\alpha = k_o\, i\, z \sin\alpha\, D^2 \qquad 2.36$$

with i representing the number of bearing rows, z being equal to the number of rolling elements in each raceway, and k_o for ball bearings being described by the following function

$$k_o = \frac{2.8}{D\sqrt[3]{(\rho_{11} + \rho_{12})(\rho_{21} + \rho_{22})}} \qquad 2.37$$

The last quantity to be defined in Equation 2.33 is g_1 which can be solved for thrust loaded bearings as

$$g_1 = \frac{F}{P_o} \qquad 2.38$$

where F is the static thrust load on the bearing in kg.

Using the above equations to calculate a value of M_1 for the MM35BS72 triplex angular contact ball bearing system under an axial load of 1000 pounds (454.5 kg), $M_1 = 1.75$ in-lb.

The total torque M can be estimated through the summation of Equations 2.32 and 2.33 such that

$$M = M_o + M_1 \qquad 2.39$$

For the MM35BS72 angular contact ball bearing operating under the aforementioned ballscrew system conditions, the total torque M was estimated to be 2.08 in-lb.

2.4 Angular Contact Ball Bearing Torque Experiment.

The angular contact ball bearing was tested to measure torques under various load conditions. The testing apparatus is capable of applying varying or static axial loads as well as varying or constant rotational speeds. This flexibility enabled the simulation of the anticipated ballscrew environment. The testing apparatus used to perform the torque tests can be seen below in Figure 2-18.

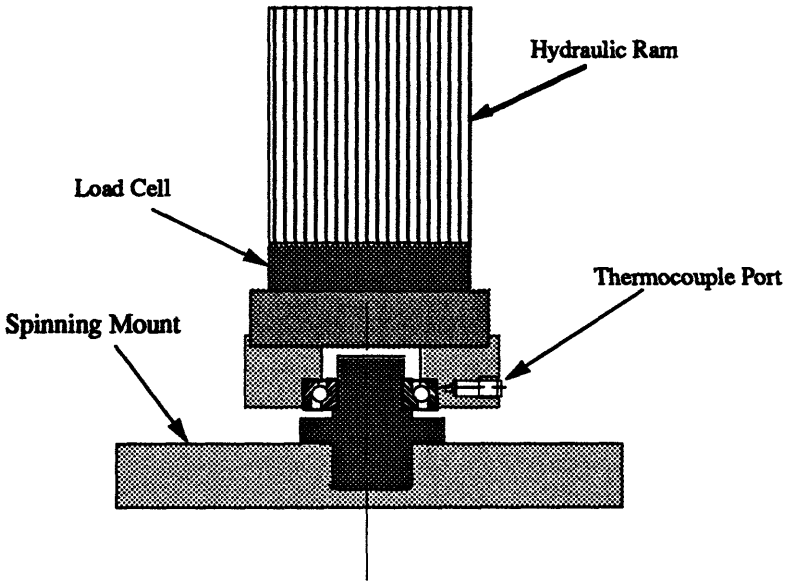

Figure 2-18. Schematic View of the Torque Test Apparatus.

The axial load is supplied by a hydraulic ram which is closed-loop controlled by a multi-axis load cell. This load cell is also responsible for reading the moment loads due to the torque of the bearing. The lubrication used was a Kluber product (Topas Isoflex NB 52) which is currently specified by the machine tool manufacturer for use on the MM35BS72 angular contact ball bearings in the ballscrew support application.

A simple program was written for the tests which coordinated the axial loading of the bearing with the rotational speed ramp-up of the spindle. The bearing was loaded prior to rotation as the preload stretch of the ballscrew in application can be thought of as a constant force on the ballscrew support bearings. In doing this, the torque test simulated a start-up while under the load of the ballscrew stretch. A worst case scenario was employed in which the bearing was subjected to the rapid traverse conditions of the machine-tool. While spinning at the equivalent rotational speed of 800ipm in the machine-tool application (1450 rpm), the axial load was varied from 500 pounds to 2000 pounds over a series of tests. The actual duty cycle that was programmed into the testing apparatus included an acceleration to 1450 rpm within one second, constant speed for four seconds and then deceleration to a complete stop.

The start-up torque curve representing the worst case torque conditions can be seen below in Figure 2-19 for varying levels of axial load. Each curve represents the average torque spike seen during the series of tests that were run on three MM35BS72 angular contact ball

bearings. The horizontal axis labelled 'Time (seconds)' has been used merely to illustrate the relative lengths of recorded torque spikes during the duty cycle.

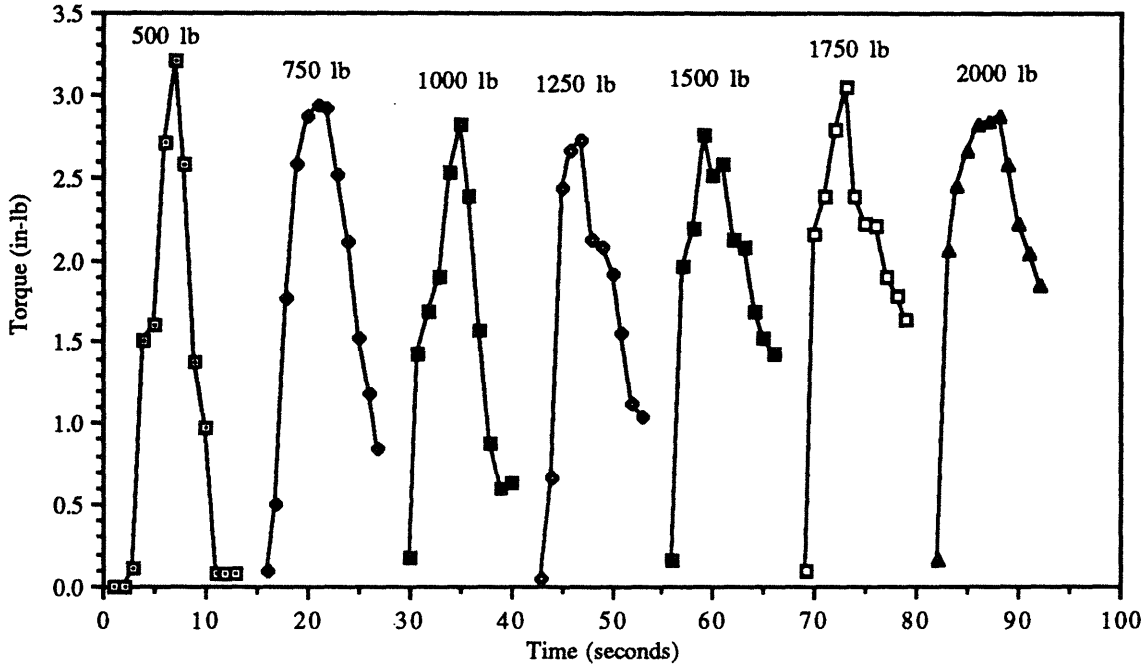

Figure 2-19. Torque Test Results for the Angular Contact Ball Bearing.

From the torque test results seen in Figure 2-19, it can be seen that the angular contact ball bearing torque spike at startup is relatively insensitive to changes in axial load. An average value that can be assigned to the MM35BS72 angular contact ball bearing for comparison purposes is 2.9 in-lb per row. Therefore, a three-row triplex stackup of this particular bearing could be estimated to have a maximum torque of 8.7 in-lb.

Referring to the end of Section 2.3, the theoretical maximum torque of the single row angular contact ball bearing was a fair approximation at 2.08 in-lb.

Although these issues will not be detailed in this study, the effects of grease volume, run-in, and usage issues all contribute to the torque characteristics of the bearing[1]. Subtle changes in lubricant amount and type as well as running-in bearings can significantly reduce wear and improve torque characteristics. Supply the bearing manufacturer with enough information so that a suitable bearing system can be chosen for the application.

---

[1] See also: T.A. Harris. Rolling Bearing Analysis. John Wiley & Sons, Inc. New York 1991.

3.0

Tapered Roller Bearing Characteristics.

The following derivation for the axial and radial deflections of tapered roller bearings can be very useful in bearing system design where axial or radial movement of the bearing under load is critical. Ballscrew actuators are such an application. The equations presented are capable of discerning deflections due to combined loading conditions in applications where the load zone encompasses all of the rollers around the raceway. It must be assumed however, that the radial and axial components of the applied load are on axis as the following derivation does not take into account tilting moments due to off-axis load components.

3.1 Axial Deflection and Stiffness Calculations.

As in the deflection calculations for angular contact ball bearings the normal deflections of the rolling elements and the raceways will be evaluated and then applied to the radial and axial directions[1]. Once again the assumption of rigid rings is used which assumes that the bearing housing and shaft are infinitely stiff so as to prevent telescoping of the inner and outer raceways. Also any frictional components resulting from interference fits within the housing or on the shaft are assumed negligible.

3.1.1 Single Row Tapered Roller Bearing.

Again, the angles of contact are critical in determining the normal deflection across the rollers. Figure 3-1 defines the two angles that will be used to calculate the axial and radial deflections for a tapered roller bearing.

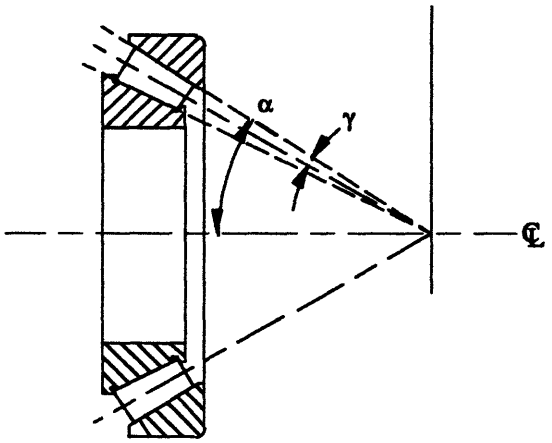

Figure 3-1. Tapered Roller Bearing Critical Angles.

α represents the 1/2 included cup angle while γ represents the 1/2 included roller angle. Defining the load zone parameter, ε, representing the combined loading condition of the

[1] See also: W. K. Dominik. "Bearing Fundamentals" copyright 1973 by The Timken Company.

bearing in application, the normal approach of the rollers and the raceways can be calculated. This can be resolved to deliver the axial and radial deflection components.

The load zone parameter can be thought of as a measure of the load zone within the bearing. When a bearing is subjected to loads that are not purely axial or radial, a combined loading reaction results. Figure 3-2 shows the differences between pure axial, pure radial, and combined loading reactions on a tapered roller bearing.

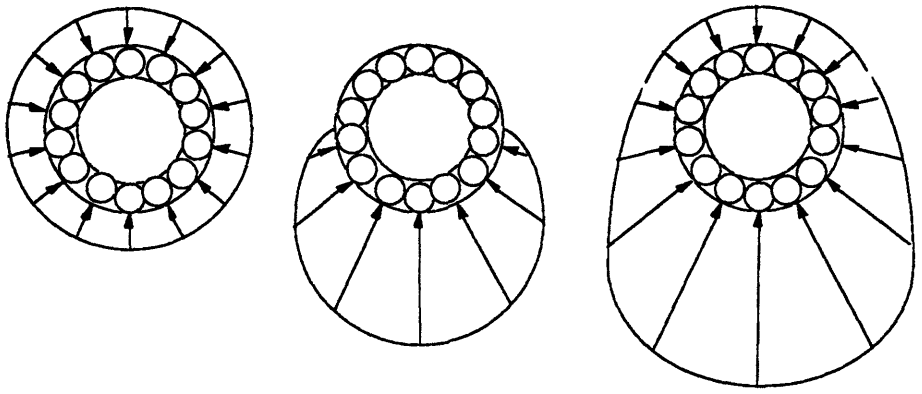

a) pure axial load b) pure radial load c) combined radial and axial load

Figure 3-2. Tapered Roller Bearing Loading Reaction Forces.

The load zone parameter, ε, is defined at the maximum loaded roller as the ratio of thrust to radial load and is related to the total radial and axial deflection components δ_r and δ_a and the 1/2 included cup angle α in the following manner:

$$\varepsilon = \frac{1}{2}\left(1 + \frac{\delta_a \tan \alpha}{\delta_r}\right) \qquad 3.1$$

For the tapered roller bearing deflection calculations, line contact is assumed to exist between the rollers and the inner and outer raceways. The rollers are also assumed to be seated squarely on the cone rib, causing the line of roller-raceway contact to fall in the same plane as the bearing's axis of rotation. When the rollers are seated squarely on the cone rib, true rolling motion will result minus any microslip conditions. If the rollers are not seated, the line of contact can no longer be guaranteed to fall along the bearing's axis of rotation and "roller skewing" can result. This causes the bearing to depart from true rolling motion into sliding friction.

A slightly different approach will be taken for the axial deflection and axial stiffness calculations for the tapered roller bearing. The method employed for the angular contact ball bearing using the curvatures breaks down for the tapered roller bearing's line contact. Instead, the tapered roller bearing's calculations will be made through the definition of the radial and axial components of the applied load. These components influence the load zone as seen in Figure 3-2. The rollers located at varying angles ψ around the bearing carry the applied load. Therefore, the sum total of the axial and radial components on each of the rollers equals the total axial and radial components of the applied load. The Hertzian relationship between the normal roller load and the resulting deformation for line contact has an exponent of 1.1 and can be seen in Equation 3.2.

$$Q_\psi = K_\psi \delta_\psi^{1.1} \qquad 3.2$$

Q_ψ is the normal load across the roller located around the raceway at angular location ψ, K_ψ is the bearing's load-deflection quantity expressed in units of lb/(in$^{1.1}$), and δ_ψ is the normal deflection across the roller at location ψ. The subscript ψ refers to the angular location of the individual rollers in the bearing raceway. Figure 3-3 illustrates the use of the roller location ψ.

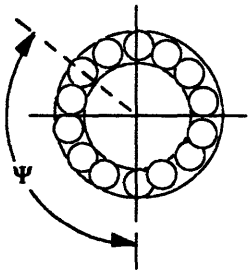

Figure 3-3. Illustration of Roller Location Angle Ψ.

From purely geometrical considerations the normal deflection across any roller δ_ψ, can be solved for in relation to the maximum normal deflection δ_n occuring at the maximum loaded roller. The following equation details the relationship between the normal deflection across any roller δ_ψ to the maximum normal deflection δ_n.

$$\delta_\psi = \left[1 - \frac{1}{2\varepsilon}(1 - \cos\psi)\right]\delta_n \qquad 3.3$$

Determination of δ_n, stems from the Hertzian relationship and is similar to Equation 3.2 for the case where $\psi = 0$.

$$Q_n = K_n \delta_n^{1.1} \qquad 3.4$$

Solving Equation 3.4 for δ_n and substituting into Equations 3.3 and 3.2 yields a relationship between the load across any roller at location ψ to the load across the maximum loaded roller:

$$Q_\psi = \left[1 - \frac{1}{2\varepsilon}(1 - \cos\psi)\right]^{1.1} Q_n \qquad 3.5$$

The sum of all Q_ψ around the raceway equals the applied load experienced by the bearing. As the normal load Q_ψ is a vector in space, it can be broken down into the axial and radial components seen in Figure 3-4.

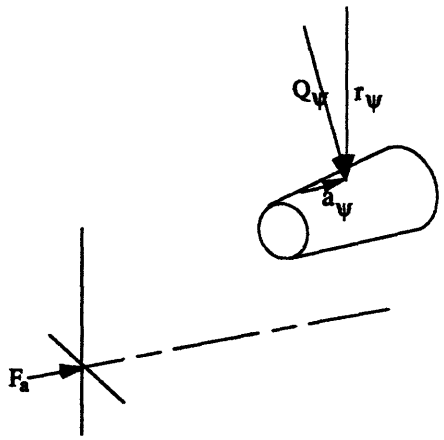

Figure 3-4. Radial and Axial Components of a Combined Loading Condition.

Vectors in space such as Q_ψ require 3 orthogonal components to be completely defined. However, in our application the net force of Q_ψ in the rotational direction is zero due to the symmetry of the load distribution. The axial and radial components a_ψ and r_ψ of Q_ψ can be expressed as

$$a_\psi = Q_\psi \sin\alpha \qquad 3.6$$

$$r_\psi = Q_\psi \cos\alpha \cos\psi \qquad 3.7$$

Substituting Q_ψ from Equation 3.5 into Equations 3.6 and 3.7, the total axial and radial force components of the applied load can be expressed as a summation of Equations 3.6 and 3.7 for all the existing roller angle locations ψ.

$$F_a = Q_n \sin\alpha \sum_{\psi} \left[1 - \frac{1}{2\varepsilon}(1 - \cos\psi)\right]^{1.1} \qquad 3.8$$

$$F_r = Q_n \cos\alpha \sum_{\psi} \left[1 - \frac{1}{2\varepsilon}(1 - \cos\psi)\right]^{1.1} \cos\psi \qquad 3.9$$

Equations 3.8 and 3.9 can be changed from summations into integrals where N is the number of rollers in the raceway. The following equations require a full complement of rollers to be accurate as the integral is evaluted using the roller locations defined by the angular location ψ.

$$F_a = Q_n \sin\alpha\, N \left\{\frac{1}{\pi}\int_0^{\psi} \left[1 - \frac{1}{2\varepsilon}(1 - \cos\psi)\right]^{1.1} d\psi\right\} \qquad 3.10$$

$$F_r = Q_n \cos\alpha\, N \left\{\frac{1}{\pi}\int_0^{\psi} \left[1 - \frac{1}{2\varepsilon}(1 - \cos\psi)\right]^{1.1} \cos\psi\, d\psi\right\} \qquad 3.11$$

The quantities within the large brackets are elliptic integrals and do not posess a direct solution through integration. Since these components describe the elliptical nature of the load components seen in Figure 3-2 c), they are termed the axial and radial integrals, J_a and J_r respectively. Equations 3.10 and 3.11 can be rewritten as

$$F_a = Q_n \sin\alpha\, N\, J_a \qquad 3.12$$

$$F_r = Q_n \cos\alpha\, N\, J_r \qquad 3.13$$

Solving both equations for Q_n delivers the following relationship.

$$\frac{J_r}{J_a} = \frac{F_r \tan\alpha}{F_a} = Z \qquad 3.14$$

From the above relationship we see that if the loading characteristics and geometry of the tapered roller bearing are known, an intermediate quantity Z representing the ratio of the radial and axial integrals is known. Remembering that

$$J_a = \frac{1}{\pi}\int_0^{\psi}\left[1 - \frac{1}{2\varepsilon}(1 - \cos\psi)\right]^{1.1} d\psi \qquad 3.15$$

$$J_r = \frac{1}{\pi}\int_0^{\psi}\left[1 - \frac{1}{2\varepsilon}(1 - \cos\psi)\right]^{1.1} \cos\psi \, d\psi \qquad 3.16$$

are both functions of the load zone parameter ε, values of ε can be iterated into Equations 3.15 and 3.16 to compute a value of Z equal to that as defined by the loading conditions in Equation 3.14. In this iteration, the load zone parameter ε describes the elliptic loading condition, much in the same way the value k represented the elliptic contact areas for the angular contact ball bearing in Section 2.1.1.

Direct integration is not available for the computation of J_a and J_r, so a simple program can be written in basic or any other computer language to evaluate the elliptic integrals using approximation techniques such as Simpson's Rule. Once values of J_a and J_r have been obtained which correspond to the load condition of the tapered roller bearing application, the normal load at the maximum loaded roller can be solved.

$$Q_n = \frac{F_a}{N \sin\alpha \, J_a} \qquad 3.17$$

Q_n represents the point normal load on the roller at the mean roller diameter. As this load is spread along the effective contact length L of the roller, Q_n' can be solved for as the load across the line of contact between the roller and the raceway.

$$Q_n' = \frac{Q_n}{L} \qquad 3.18$$

From this the normal deflection δ_n can be calculated.

$$\delta_n = 8.89e^{-8} Q_n' \left[8.45 + \log\left(\frac{\sin\gamma}{D\, Q_n' \sin\alpha}\right)\right] \qquad 3.19$$

where D is the mean roller diameter. Once the normal deflection has been solved for, the axial and radial deflection components can be resolved through the use of the load zone parameter ε.

$$\delta_r = \left(\frac{1}{2\varepsilon}\right)\frac{\delta_n}{\cos\alpha} \qquad 3.20$$

$$\delta_a = \left(1 - \frac{1}{2\varepsilon}\right)\frac{\delta_n}{\sin\alpha} \qquad 3.21$$

Using the above equations to calculate the axial deflection of the tapered roller bearing under different axial load conditions, the axial stiffness can be found by analyzing the resulting load-deflection curve.

The following schematic details the calculation procedure for the axial and radial deflections of a tapered roller bearing. The system characteristics are listed in the circles while the calculated values are located in the squares.

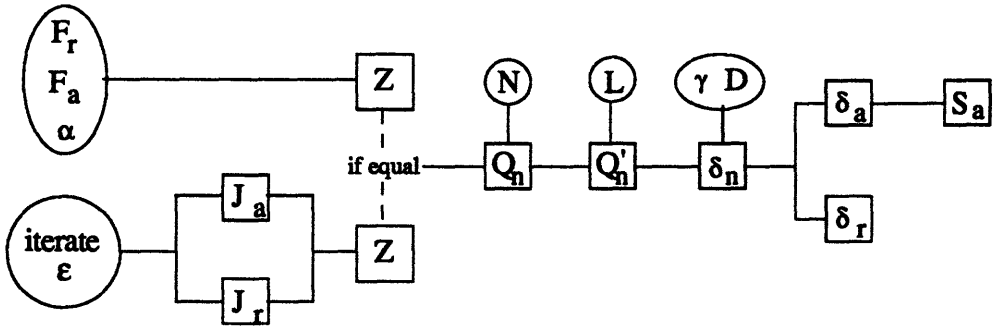

3-5. Schematic of Tapered Roller Bearing Calculations.

Using the above flowchart, a spreadsheet can be constructed to perform the calculations for the tapered roller bearing in thrust loaded applications as was done for the angular contact ball bearing.

Tapered Roller Bearing Deflection Calculator
units: in, lbf, and degrees

Load Conditions:	Tapered Roller Bearing Parameters:
radial load (lb) = 1.0	1/2 incl. cup angle (°) = 30.8
axial load (lb) = 2040.0	number of rollers = 16.
	eff. roller length (in) = 0.49
	1/2 incl. roller angle (°) = 4.00
	mean roller diameter (in) = 0.33

Intermediate Calculations:

Z = 0.000292216 loading condition
Ja = 0.998677060 Sjovall's Axial Thrust Integral
Jr = 0.000296737 Sjovall's Radial Thrust Integral
E = 845.091052717 Epsilon (load zone factor)

Axial Deflection: 0.000466 0 inches
Radial Deflection: 0.000000 2 inches

Figure 3-6. Tapered Roller Bearing Deflection Calculation Spreadsheet.

Using the above calculation procedures and the spreadsheet seen in Figure 3-6, a load-deflection curve can be generated from which the axial stiffness of the bearing can be taken.

The load-deflection curve will result in a straight line. This stems from the contact area formed between the rollers and the raceways. The contact area for the tapered roller bearing is elliptical in nature, but the rate of elliptical deviation with increasing load is very small as a result of the line contact across the raceway prior to deformation. This is in contrast to the point contact of the angular contact ball bearing. The taper's ellipse is very long, while the balls' is much more circular in nature. Hence, the change in elliptical contact area for a tapered roller bearing lies mostly along one axis as opposed to two for the angular contact ball bearing. This delivers an approximately linear stiffness relationship for the tapered roller bearing instead of a much more complex relationship as seen for the angular contact ball bearing.

A good first order approximation of roller bearing axial deflection has been presented in Harris' Rolling Bearing Analysis[1]. This approximation allows quick back-of-the-envelope estimations of axial deflection which can be used to create a load deflection curve to determine rough stiffness values.

$$\delta_a = 8.71 \times 10^{-7} \frac{Q^{0.9}}{L^{0.8} \sin \alpha} \qquad 3.22$$

In this equation, $Q = F_a/(N \sin\alpha)$ with the axial load, F_a, in lbs and the effective length, L, in inches.

Approximations for the contact areas that are formed at the roller-raceway and rib-roller interfaces can be used for heat generation approximations. The resulting contact areas of the tapered roller bearing will be compared with those formed by the angular contact ball bearing. It will be assumed that neither the rollers or the raceways are crowned and that line contact exists. This creates the situation in Hertzian deformation analysis concerning curved surfaces where the radii corresponding to the line contact of the roller and raceway are infinite. To begin, the normal load at the inner raceway must be known and can be found through the following equation:

$$Q_i = \frac{F}{Z \sin(\alpha - 2\gamma)} \qquad 3.23$$

Here F is equal to the applied axial load on the bearing in pounds, Z represents the number of rollers and the quantity $(\alpha\text{-}2\gamma)$ solves for the 1/2 included cone angle.

Working with the assumption of no crown on the roller or raceway, the relationship established for the summation of the curvatures becomes:

$$\Sigma p_i = \frac{1}{D\left(1 - \frac{D \cos(\alpha - 2\gamma)}{d_m}\right)} \qquad 3.24$$

---

[1] T. A. Harris. Rolling Bearing Analysis. John Wiley & Sons, Inc. New York 1991. pg. 329

where D represents the mean roller diameter in inches, and d_m is the pitch diameter of the bearing inches. As line contact exists across the raceway, the semimajor axis, a, of the contact ellipse is equal to 1/2 of the effective contact length, L.

$$a = 0.5\,L \tag{3.25}$$

The semiminor axis, b, can be solved through the following relation:

$$b = 0.000278\left(\frac{Q_i}{L\,\Sigma p_i}\right)^{\frac{1}{3}} \tag{3.26}$$

The elliptical contact area is then solved for the roller-raceway contact area as:

$$A = \pi ab \tag{3.27}$$

The maximum stress along the inner raceway can also be solved for:

$$\sigma_{max} = \frac{2\,Q_i}{\pi\,L\,b} \tag{3.28}$$

Using the above equations and applying them to the tapered roller bearing defined in Figure 3-6:

$a = 0.245$ in
$b = 0.003827$ in
$A = 0.000938$ in^2
$\sigma_{max} = 112{,}000$ psi

To solve for the contact area at the rib-roller interface for the case where the rollers have spherical ends and angled rib geometries, the actual contact can be modelled as that of a sphere and a cylinder. Let the sphere radius equal the roller spherical end radius and the cylinder radius equal the radius of curvature of the conical flange at the statistical mean point of contact. With the knowledge of the elastic contact load, material properties, and geometries, the resulting deflections and stresses can be calculated. For the rib-roller end, the following have been calculated in reference to the bearing in Figure 3-6:

$a = 0.075$ in
$b = 0.017$ in
$A = 0.001275$ in^2
$\sigma_{max} = 60{,}000$ psi

Comparing the results of the contact areas with those from the angular contact ball bearing in Section 2.1:

	tapered roller bearing	angular contact ball bearing
Elliptical area in rolling contact	0.030 in^2	0.234 in^2
Elliptical area in sliding contact	0.020 in^2	-

The above values were solved for by taking the calculated elliptical contact areas and multiplying them by the number of rolling elements. Both inner and outer raceway contact areas were used in the above tabulation. Although the tapered roller bearing appears to have substantially less area in contact, the sliding friction component that exists at the rib-roller interface is extremely significant torque and heat generation as will be examined later.

3.1.2 Two-Row Tapered Roller Bearings.

When designing tapered roller bearings into an assembly certain issues must be addressed. Included are issues of lubrication, required finishes, axial and radial runout, fits or clearances, preloads and endplay, mounting schemes, and operating conditions. The bearing manufacturer is the best source of guidance on these issues and can often recommend several viable alternatives.

In designing a tapered roller bearing to perform with similar characteristics as an angular contact ball bearing in ballscrew support applications, all of the above issues had to be approached. One important design constraint used in the design was the desire for the tapered roller bearing support package to function within the angular contact ball bearing housing. This allows the evaluation of the experimental tapered roller bearings in applications already using angular contact ball bearings. Referring back to Figure 2-12, the bearing housing can be seen. As there is only one shoulder on which to seat the outer raceway or cup of the tapered roller bearing, a direct mount was employed. Figure 3-7 shows two single rows of tapered roller bearings mounted in 'direct' fashion.

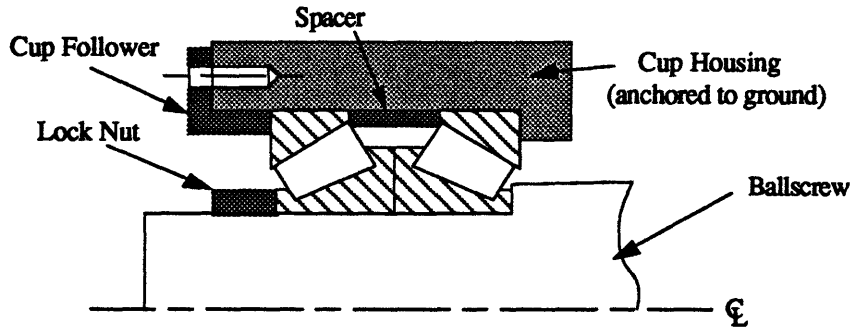

Figure 3-7. Tapered Roller Bearing Direct Mounting Scheme.

The dark component between the cups of the bearings is a spacer. This spacer is used to set the amount of preload or endplay that the bearing assembly experiences when mounted in the application. Pre-load was discussed earlier in Section 1.2.3. Endplay is a bearing setting in which the rollers and raceways are not in contact with one another when the bearing is mounted. A spacer used in a preloaded, direct mounting application is undersized; causing elastic deformation of the rollers and raceways to take place until the bearing cups are seated against the spacer and the stationary shoulder of the application. An endplay application would use an oversized spacer such that thermal growth during operation will bring the bearing into a preloaded condition.

In Figure 3-7 the tapered roller bearings are mounted in direct fashion. In this mounting scheme the lines of contact converge upon one another when drawn towards the axis of rotation. Figure 3-8 shows both an indirect mount and a direct mount with the contact lines extended down crossing the axis of rotation.

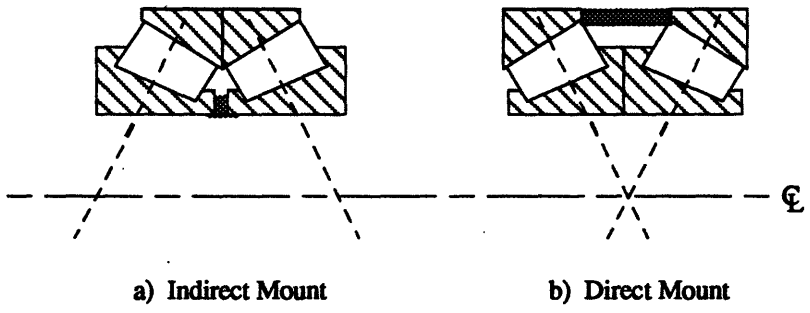

Figure 3-8. Indirect and Direct Mounts.

An advantage of the indirect mount can be seen in Figure 3-8. Contrary to directly mounted bearings, increases in temperature across indirectly mounted bearings allow the expansion of the components such that the rollers do not get 'pinched'. However, in ballscrew applications, the duty cycle of the bearings is moderate at best and hardly poses a threat to the thermal stability of the bearings. As a precautionary measure, the spacer that sets the preload within the directly mounted tapered roller bearings can be undersized to allow for a certain amount of thermal expansion to take place within the bearing.

In light of the above information concerning some of the differences between the direct and indirect mounting styles of tapered roller bearings, the direct mounting decision was pursued based upon additional information. Constrained by the angular contact ball bearing envelope, the axial stiffness of the tapered roller bearing was maximized by taking a roller and sweeping it on apex to allow for a higher contact angle and better axial load carrying capability. In doing so, the indirect mounting configuration required a cone spacer within the bearing as well as cup spacers outside the bearing to clear the cage and seat within the ball bearing housing. Since the rollers were swept up to such a steep angle, the thin section of the cup necessitated a spacer that was too thin to accommodate the axial loads without the risk of buckling. Therefore, the direct mount was used allowing the bearings to seat in the ball bearing housing using the wide section side of the cup.

The axial stiffness calculation procedure for the back-to-back, or direct, mounting of the tapered roller bearing is very similar to that for the triplex angular contact ball bearings. For the two-row tapered roller bearing, the total stiffness is the sum of the stiffnesses of the individual rows within the bearing. The bearing stiffnesses are summed in parallel as the perfect load sharing assumption is made. This is a fair assumption as the inner raceways of the two rows of tapered roller bearings are constrained to move as a single unit by the locknut operating against the outside most bearing (Refer to Figure 3-7). This can be illustrated by modelling the two rows of tapered roller bearings as springs.

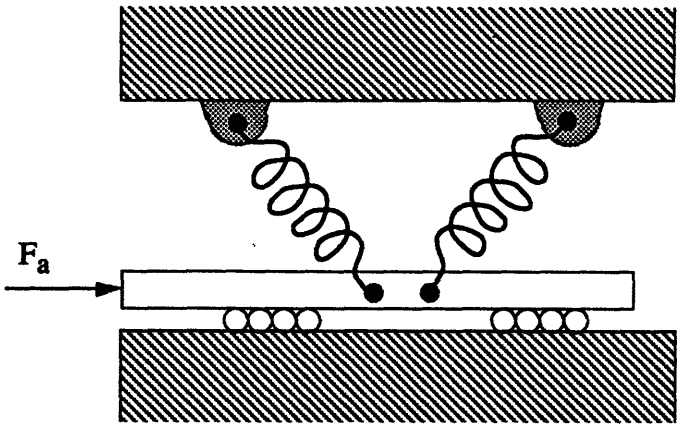

Figure 3-9. Two-Row Tapered Roller Bearing Spring Model.

When solving for the two-row stiffness values, the preload within the system must be taken into account. Any load in addition to the preload will effect the loads that are carried by the two bearings. Because the tapered roller bearings are in line contact, their axial stiffness values do not change appreciably with changes in load. The insensitivity of the tapered roller bearing to changes in load can be seen as one traverses the load deflection curves. The tapered roller bearing curve is linear in nature while the curve for the angular contact ball bearing is not. This makes stiffness predictions difficult for the angular contact ball bearing, especially in dynamic systems where operating conditions and temperatures are varying.

3.2 Tapered Roller Bearing Axial Deflection Experiment.

The axial deflection measurements for the tapered roller bearing were performed in the same manner as for the angular contact ball bearing. Three ball-tipped styluses were used to measure the axial deflection of the bearing under an increasing axial load. The setup used for the tests can be seen in Figure 3-10.

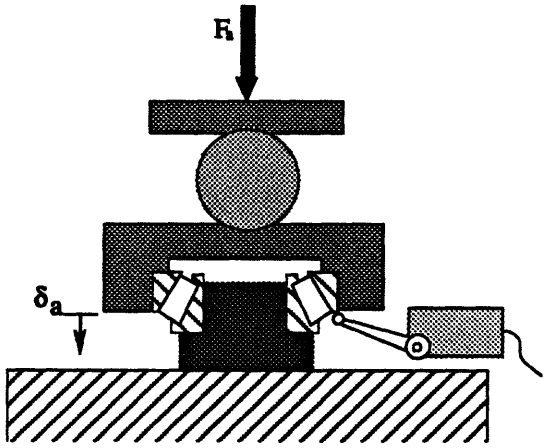

Figure 3-10. Tapered Roller Bearing Axial Deflection Setup.

The test method was identical to that used for the angular contact ball bearing and can be found in Section 2.2. Figure 3-11 shows a resulting axial deflection curve for the tapered roller bearing.

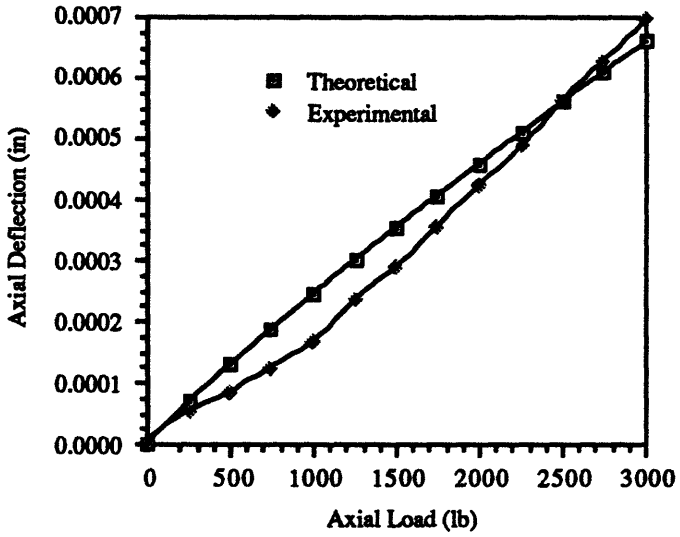

Figure 3-11. Comparison of Theoretical and Experimental Axial Deflection Data.

The slope of the experimental curve is essentially linear as the theory outlined in Section 2.1 predicts. The resulting inverse of the slope of the load-deflection curve delivers a value of 3.60×10^6 in/lb.

The nonlinearity that appears at the lower end of the load-deflection curve can be attributed to the innaccuracy stackup of the test procedure. As with the angular contact ball bearing,

the test bearing was placed within the fixture seen in Figure 3-10 and the resulting deflections recorded. After this, the bearing was removed and the fixture deflection was recorded over the same loading range. The fixture curve was subtracted from the test curve delivering the true bearing deflection curve seen in Figure 3-11. The three point averaging system employed for the axial deflection measurements has a built in gauging variation that is increasingly sensitive with decreasing load. This inherent innaccuracy is compounded by the fact that the two curves, each with their own tolerances are subtracted from one another to deliver the true tapered roller bearing deflection.

3.3 Tapered Roller Bearing Torque Calculations.

As with the angular contact ball bearing, the torque characteristics of the prototype tapered roller bearing have been predicted theoretically[1].

There are two components of frictional torque within a bearing that we must concern ourselves with for the ballscrew application. These are the frictional resistances that occur at the rib-roller interface and at the roller-raceway interface. It will be assumed that due to the low operating speed of the ballscrew application that the effects of viscous drag on the rollers due to lubricant churning effects can be ignored and that the roller-raceway frictional effects are much larger than the roller-rib frictional effects.

The running torque within a tapered roller bearing is defined as the rotational resistance of the bearing under operating conditions. As with the angular contact ball bearing, this depends on many factors: geometry, loading, the number of rollers, rotational speed, and lubricant viscosity. The running torque equations that will be presented are for bearings whose torque values have stabilized after a period of operation known as a 'run-in' time. The presented equations are primarily geared towards oil recirculated systems, however these equations also serve as a conservative estimate of operating torque for bearings using grease or oil mist systems as their means of lubrication. In grease packed systems, such as the ballscrew application, the running torque will tend to be slightly lower than that for oil fed systems, however, the operating temperature may be slightly higher due to the slower rate of heat dissipation.

---

[1] "Bearing Torque, Heat Generation, and Operating Temperature". copyright 1984 by The Timken Company

For pure thrust load situations, an estimate of the bearing running torque can be calculated from the following equation:

$$M = 3.54 \times 10^{-5}\ G_1\ (n\ \mu)^{0.62}\ F_a^{0.30} \qquad 3.29$$

M is the operating torque of the tapered roller bearing in units of in-lb, G_1 is a bearing geometry factor supplied by the manufacturer, n is the rotational speed in rpm, μ is the lubricant viscosity in centipoise, and F_a is the applied thrust load in pounds. Equation 3.29 will underestimate the running torque if the operating speed, n, is less than n_{min} which can be calculated from

$$n_{min} = \frac{1700\ F_a^{.67}}{G_2\ \mu} \qquad 3.30$$

G_2 is a bearing geometry factor supplied by the manufacturer.

Equations 3.29 and 3.30 conservatively estimate the running torque for a single row tapered roller bearing as 10.67 in-lb under ballscrew application conditions of 1450 rpm, F_a=1500 lb, and using a centipoise equivalent for the 27 Cst value of the grease lubricant at a theoretical operating temperature of around 130°F.

3.4 Tapered Roller Bearing Torque Experiment.

The tapered roller bearing was tested to measure torques under various load conditions. The same testing apparatus was used as in Section 2.4 for the angular contact ball bearing and can be seen in Figure 3-12.

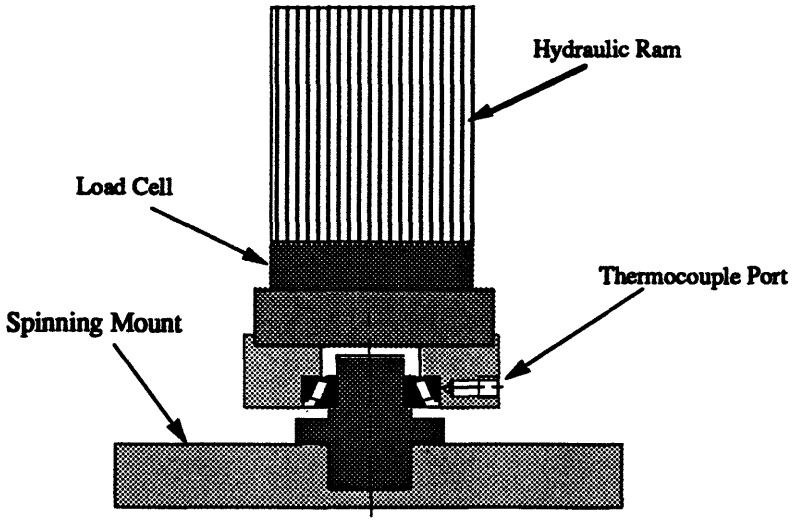

Figure 3-12. Torque Test Setup for Tapered Roller Bearing.

The bearings were lubricated with the same Kluber product as was specified for the angular contact ball bearings for use in the ballscrew support application.

The same duty cycle was run on the tapered roller bearings and the resulting torque spikes taken from the test results can be seen in Figure 3-13.

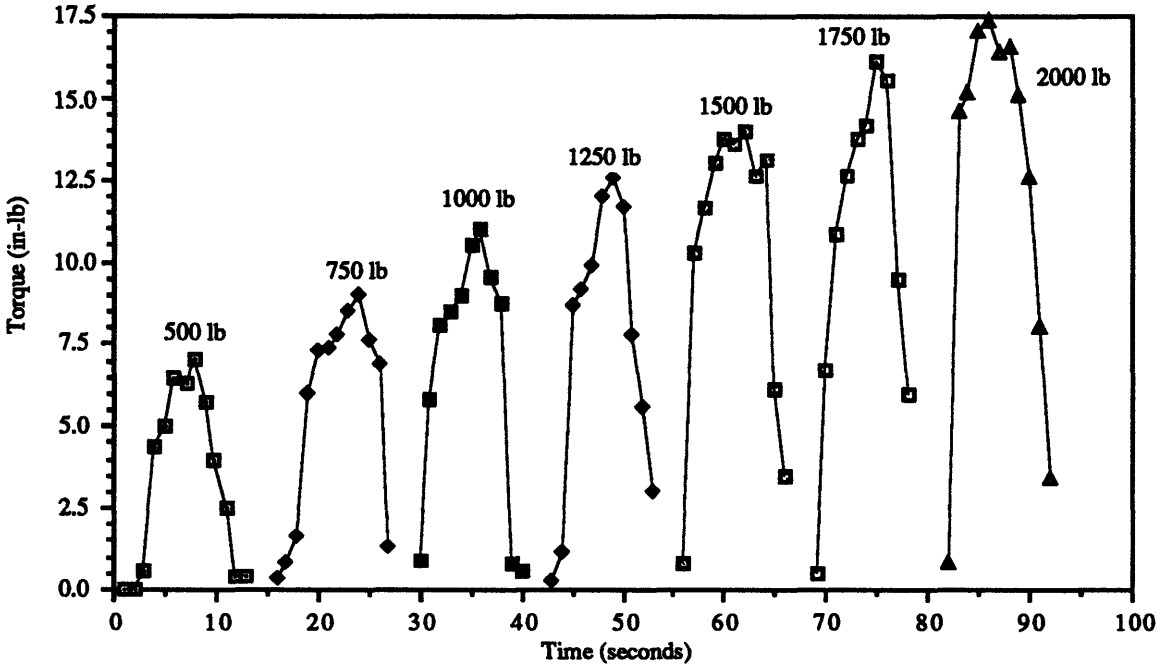

Figure 3-13. Torque Test Results for the Tapered Roller Bearing.

As in Section 2.4, each curve represents the average torque spike seen during the series of tests that were run on three tapered roller bearings. The horizontal axis labelled 'Time (seconds)' has been used merely to illustrate the relative lengths of recorded torque spikes during the duty cycle.

From the torque test results seen in Figure 3-13, it can be seen that the tapered roller bearing torque spike at startup is sensitive to changes in axial load. This is anticipated as the increasing axial load creates a force at the rib-roller interface along the cone due to the geometry of the bearing. This rib load increases the heat generation of the bearing as the rib-roller interface is in sliding contact as opposed to the roller-raceway interface where rolling motion is prevalent.

An average value that can be assigned to this tapered roller bearing for comparison purposes is 14.0 in-lb per row. This value was taken from the 1500 pound axial load worst case torque spike seen above in Figure 3-13 as the application is using a 1500 pound preload across the bearings. Therefore, a two-row stackup of this particular bearing could be estimated to have a maximum torque of 28.0 in-lb.

Referring to the end of Section 3.3, the theoretical maximum torque of the single row tapered roller bearing 10.67 in-lb was a fair approximation of the application conditions of 14.0 in-lb.

Again, the issues of bearing run-in, special lubrications, and usage issues all tie into the global torque-minimization effort which are best addressed by the bearing manufacturer.

A single row comparison of the angular contact ball bearing torques and the tapered roller bearing torques can be seen in the following table and will be detailed further in Section 4.3.

	angular contact ball bearing	tapered roller bearing
theoretical torque	2.08 in-lb	10.67 in-lb
experimental torque	2.9 in-lb	14.0 in-lb

4.0

Ballscrew System Characteristics.

This section deals with the stiffness and torque characteristics associated with ballscrew systems. Position intensive operations demand stiff, low torque actuators. The stiffer the axis, the more conducive the axis is to precise positioning via upper-level control schemes. Incorporating a stiffer axis onto a machine-tool bed for actuation of a turret head or table, more accurate part trajectories will be realized along with closer tolerancing of final dimensions due to the lack of 'give' in the system. Low torque applications are also favored as they reduce the amount of energy used, minimizing temperature induced precision loss.

4.1 Ballscrew Stretch Theory.

Pre-tensioning a ballscrew enables the ballscrew system to improve its axial stiffness and to better deal with the thermal growth that arises during extended, aggressive operation.

Ballscrew actuators are subject to thermal gains during operation due to the frictional-torque of the preloaded balls within the ballnut and the preloaded support bearings. The transfer of heat to the ballscrew causes the ballscrew to expand in all unconstrained directions. Knowing the thermal coefficient of expansion for steel ($\alpha = 6 \times 10^{-6}/^{\circ}F$) and the relationship between temperature change and induced thermal strain, ε_t,

$$\varepsilon_t = \alpha (T - T_o) \qquad 4.1$$

a percentage change in the dimensions of the ballscrew can be estimated. Restricting ourselves to the strain that occurs along the rotating axis of the ballscrew, it is apparent that temperature changes directly effect the mechanical positioning accuracy of a ballscrew system. The thermal growth alters the length between adjacent threads along the ballscrew, causing an error in the translation of rotational position into linear position. Therefore, the position of the carriage will not be able to be determined accurately from the rotary encoder unless the carriage position is monitored by an alternate form of position feedback. As linear scales and laser interferometer systems are not cheap or conducive to aggressive manufacturing environs, pre-tensioning of the ballscrew has become an inexpensive alternative to increase positioning capability.

Ballscrew pre-tensioning, or stretching, induces an elastic strain within the ballscrew that opposes the thermal strain that develops during operation. Consider the basic elastic strain along the axis of the ballscrew ε_e:

$$\varepsilon_e = \frac{\Delta L}{L} \qquad 4.2$$

Equation 4.2 is the relationship of the increase in axial length of the ballscrew ΔL, to the initial length of the ballscrew L. The total system strain in the axial direction can be expressed as a combination of the elastic and thermal strain components.

$$\varepsilon_{total} = \varepsilon_e + \varepsilon_t \qquad 4.3$$

When the elastic strain is applied by stretching the ballscrew, a fixed-fixed condition is created as both ends of the ballscrew are supporting the load due to the stretch. This load F_{strain} can be solved for:

$$F_{strain} = \varepsilon_{total} E A \qquad 4.4$$

The cross-sectional area of the ballscrew at the thread groove base diameter should be used to calculate A, and the Young's Modulus, E, for steel is 30×10^6 psi. As the ballscrew warms up, the thermal component of Equation 4.3 increases, changing the load F_{strain} that exists at the support bearings. Remember that the load F_{strain} is in addition to the preload F_p that is ground into the bearings by the manufacturer. The total load that exists across the support bearings is critical in the case of the angular contact ball bearing as it directly influences the axial stiffness as was seen in Section 2. In comparison, the tapered roller bearing axial stiffness is linear due to the line contact that exists between the roller and the raceways and is relatively insensitive to changes in axial load. To calculate the load that exists across the support bearings, refer to Section 2.1.2 (pg. 28) where the forces due to the stretch and the thermal growth can be modelled as externally applied loads.

Consider the triplex and tapered roller bearing mounting conditions in Figures 2-12 and 3-7. When the total system strain (Equation 4.3) equals zero, the thermal and elastic strains will be equal. This implies that the ballscrew has expanded to the point where it is overcoming the force of the stretch that was applied to the ballscrew. Depending upon the mounting scheme employed on the ends of the ballscrew, this will do one of two things. The increasing thermal strain will either unseat the support bearings from the shoulders within the housings, or in the case where the outer raceways of the bearings are retained in the housings, the ballscrew will undergo compressive loading which will affect the rotational accuracy of the ballscrew as it begins to buckle.

In the case where the preloaded support bearings are held against the shoulder of the housing by the stretch load applied to the ballscrew, should the thermal strain be such that the bearings unseat themselves from the housing, they will retain their preload. The bearing packages retain their preload as they are tightened along the shaft to the shoulder of

the ballscrew in a configuration that does not allow them to move axially, relative to one another.

Should the thermal strain equal the induced elastic strain in the case where the support bearings are rigidly constrained, the ballscrew changes from a fixed-fixed mounting to a fixed-supported mounting. The significance of which is very important when calculating the ballscrew axial stiffness as will be seen in Section 4.2.

The ballscrew being used in the application evaluation of the two support bearing packages has the following basic characteristics:

supported length	52"
thread groove base diameter	1.378"
mounting condition	fixed-fixed
pre-tensioning stretch	0.0015"

From this information the elastic strain ε_e can be calculated as 2.88×10^{-5}. Remembering that $F = \varepsilon EA$, the system force resulting from the stretch is solved to be 1290 lbs. Therefore, each of the two support bearing packages must absorb 645 lbs axially. To cause the support bearings to disengage with the housing shoulders, a change in temperature ΔT must occur that translates into an ε_t having an equivalent force greater than 1290 lbs. Using Equations 4.1 and 4.4, ΔT is found to equal 4.8°F.

ε_e	2.88×10^{-5}
ΔT to overcome ε_e	4.8°F

Remember that the change in temperature of 4.8°F is assessed as a uniform temperature throughout the ballscrew. There are four points of heat generation, the ballnut, the motor, and the two support bearing packages. The heat accumulation within the ballscrew that leads to thermal growth is governed by a number of factors including: ballnut and support bearing lubrication, duty cycle, traversing speeds, conduction through the bearing housings, motor mounting, and environmental conditions.

4.2 Ballscrew System Axial Stiffness.

Before a ballscrew is designed into an application for use as a linear positioning element, it is necessary to make an initial approximation of the actuator's stiffness. An actuator that

does not possess enough stiffness will be susceptible to lost precision and productivity. By evaluating the individual elements of the ballscrew actuator one piece at a time, a system stiffness can be calculated. Take the following actuator composed of ballscrew, ballnut, support bearings, and bearing housings.

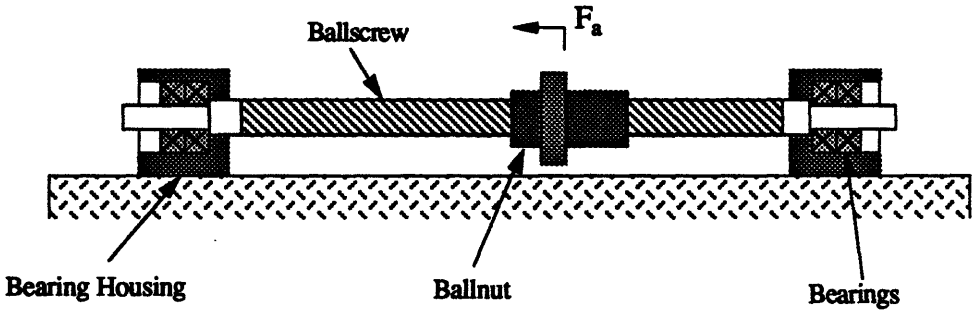

Figure 4-1. Ballscrew System.

Each of these components has an inherent stiffness which can be lumped together with the other elements to solve for the system stiffness. Consider the force-flow for the fixed-fixed ballscrew system. When an external force F_a, is applied to the carriage which is kinematically linked to the ballnut, only the axial component of that force is transferred through the ballscrew system. The reaction of the axis to the applied axial load is dependent upon the inherent stiffnesses of the axis components, the ballnut position, and the system temperature. Modelling the axis components as a series of springs, Figure 4-2 evolves.

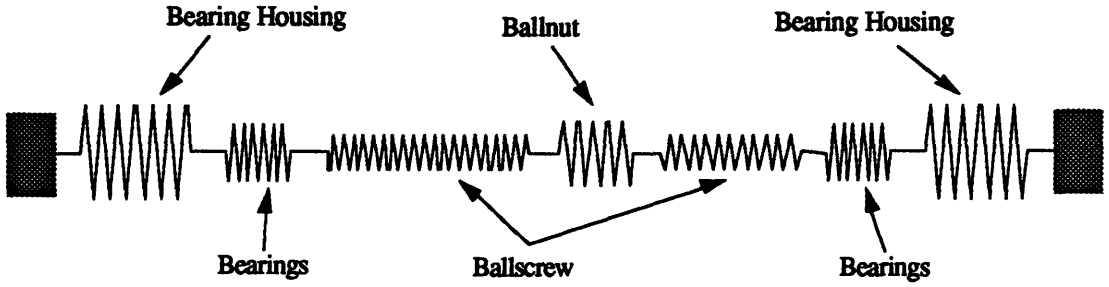

Figure 4-2. Ballscrew System Spring Model.

The system stiffness can be calculated by summing the individual stiffness values in series.

$$\frac{1}{S_{system}} = \frac{1}{S_{housing}} + \frac{1}{S_{bearings}} + \frac{1}{S_{ballnut}} + \frac{1}{S_{ballscrew}} + \frac{1}{S_{bearings}} + \frac{1}{S_{housing}} \qquad 4.6$$

Knowing the stiffness of the actuator, axial deflections can be calculated for given loading conditions. To illustrate the loading conditions that exist in the stretched ballscrew system, consider Figure 4-3.

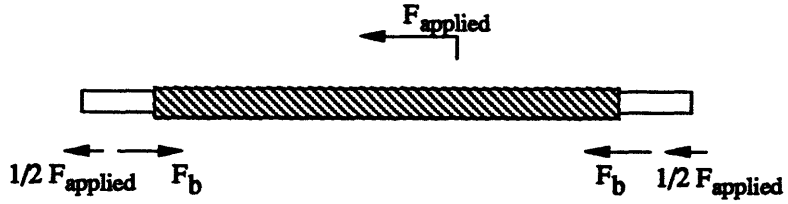

Figure 4-3. Stretched Ballscrew System Free Body Diagram

In the above figure, the applied load $F_{applied}$ is seen acting at a point along the length of the ballscrew defined by the ballnut position. The resulting loading conditions at the support bearing locations are also shown. The force F_b is representative of the load that exists across the bearings due to the preload, ballscrew stretch, and any thermally induced strains. Knowing the applied force $F_{applied}$ and the system forces on the support bearings, F_b, these can be combined to solve for the actual bearing load conditions that exist. Subsequently, the stiffnesses for the individual rows of the support bearing can be computed and then combined in parallel under the perfect load sharing assumption to represent the support bearing stiffness. Consider the following example:

Using the angular contact ball bearings in triplex fashion and the tapered roller bearings in a two-row direct mount, the loads across each of the bearings on both ends of the ballscrew will be tracked as the bearing are preloaded, stretched with 1290 lbs of axial load (645 lbs per end), and subject to an applied axial load of 1000 lbs. The applied axial load is oriented such that it acts towards the left set of support bearings as in Figure 4-3. The numbers entered for each end of the ballscrew correspond to the load across the different rows of bearings at each end. Hence the triplex set of angular contact ball bearings has three entries while the two-row tapered roller bearing has two.

	angular contact ball bearings		tapered roller bearings	
	ballscrew left end	ballscrew right end	ballscrew left end	ballscrew right end
preload condition	1020,1020,2040	2040,1020,1020	1500,1500	1500,1500
after ballscrew stretch	1343,1343,1395	1395,1343,1343	855,2145	2145,855
under the applied load	1093,1093,1895	895,1593,1593	1355,1645	2645,355
stiffness per row $\times 10^6$	3.15,3.15,3.79	3.05,3.54,3.54	3.60,3.60	3.60,3.60
support bearing stiffness	10.09×10^6	10.13×10^6	7.2×10^6	7.2×10^6

The example does not incorporate any thermal effects. If any were present, an additional line would be entered in the above example between the ballscrew stretch and the applied load. The stiffness values listed at the end of the example are the final stiffness values of the support bearing packages under the perfect load sharing assumption. The preload conditions for the angular contact ball bearings were determined by observing the load-deflection curves that were generated experimentally in Sections 2.2. The tapered roller bearing preload was created to match the single angular contact ball bearing preload of 1500 lb. The stretch load was calculated in Section 4.1 and the applied load was detailed in Section 4.2.

The theoretical stiffnesses for the components of the ballscrew system to be used in the experimental machine-tool axis are listed below:

	angular contact ball bearings	tapered roller bearings
left support bearing package stiffness	10.03×10^6 lb/in	7.20×10^6 lb/in
right support bearing stiffness	10.03×10^6 lb/in	7.20×10^6 lb/in
minimum ballscrew stiffness	3.44×10^6 lb/in	3.44×10^6 lb/in
minimum ballnut stiffness	5.50×10^6 lb/in	5.50×10^6 lb/in

The support bearing values listed above reflect the package bearing stiffness on each end of the ballscrew due to the preload and stretch. The stiffness calculations for the ballscrew and ballnut can be found in Sections 4.2.1 and 4.2.2 respectively. Returning to Equation 4.6, the total axis stiffness can be solved.

$$\frac{1}{S_{total}} = \frac{2}{S_{bearings}} + \frac{1}{S_{ballscrew}} + \frac{1}{S_{ballnut}}$$

Without any deviation in temperature from the time the ballscrew stretch was applied and ignoring any externally applied loads:

S_{total} with 6 rows of angular contact ball bearings = 1.48×10^6 lb/in

S_{total} with 4 rows of tapered roller bearings = 1.33×10^6 lb/in

The above system stiffness calculation reveals that the tapered roller bearing can provide similar system stiffness with fewer rows. This translates into a cost savings when using the tapered roller bearings instead of the triplex angular contact ball bearings. For a two

axis machine where 12 angular contact ball bearings would be used, only 8 tapered roller bearings would be necessary.

Another advantage of the tapered roller bearings is the linear load-deflection curve. With tapered roller bearings used as the ballscrew support bearings in a machine-tool axis, their will be less change in system stiffness under dynamic operating conditions. A perfect application for tapered roller bearings would be in a crossed axis application where axis-reversal loads can significantly effect the final part geometry. By using tapered roller bearings in such an application, the system stiffness will not change during axis-reversal enabling more accurate trajectories and better finishes.

4.2.1 Ballscrew Axial Stiffness.

Ballscrew axial stiffness is dependent upon the end-fixity conditions. There are two standard types of mounts: fixed-fixed and fixed-supported. In fixed-fixed mounts both support bearing packages are constrained from moving axially. These types of mounts are used in machine tools on axes that are subject to varying forces and require accurate positioning without the use of carriage position feedback. By fixing both ends of the ballscrew using an applied stretch, the rotational frequency is improved due to the fixity conditions. This allows faster actuation with less rotational error. Fixed-supported mounts are traditionally employed on ultra-precision measuring machines where carriage forces are minimal and carriage position feedback is employed. In these types of applications, the tail end of the ballscrew free to move axially, hence expansion does not affect the positioning or rotational accuracy.

Fixed-Fixed Axial Stiffness.

The axial stiffness of the fixed-fixed condition can be solved using the following relationship.

$$S_{a\ \text{fixed-fixed}} = \frac{AEL}{x(L-x)} \qquad 4.7$$

A represents the cross-sectional area of the ballscrew at the bottom of the thread, *E* is the Young's Modulus, *L* is the length of the ballscrew, and *x* is the position of the ballnut

along the ballscrew. The maximum axial deflection occurs when the ballnut is at the middle of the ballscrew in a fixed-fixed condition. Therefore the minimum stiffness through Equation 4.7 is found when $x=L/2$.

The minimum stiffness of the ballscrew used in the ballscrew test rig was solved using Equation 4.7 and found to equal $3.44x10^6$ *lb/in.*

Fixed-Supported Axial Stiffness.

The axial stiffness in the fixed-supported state is much less than that in the fixed-fixed condition.

$$S_{a\ \text{fixed-supported}} = \frac{AE}{x} \qquad 4.8$$

As the ballscrew is rigidly supported on only one side, the distance x from that side determines the axial stiffness of the fixed-supported ballscrew.

Figure 4-4 demonstrates the axial stiffness of a 52" long ballscrew when employed in both the fixed-fixed and fixed-supported mounting conditions as a function of ballnut position.

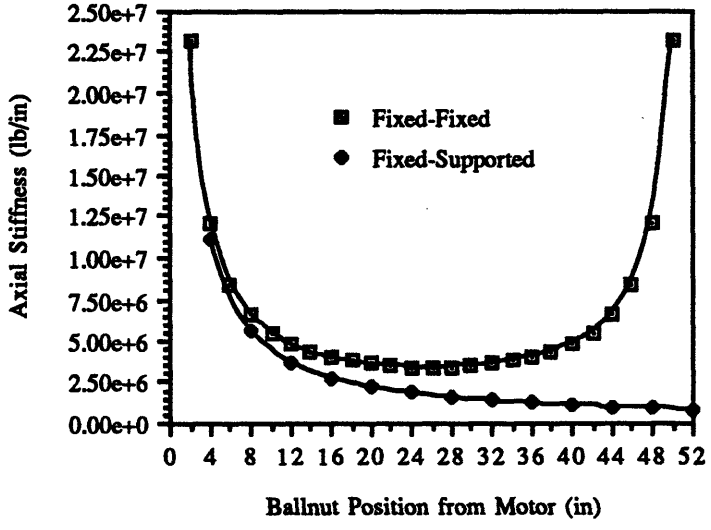

Figure 4-4. Ballscrew Stiffness as a Function of End-Fixity and Ballnut Position.

In estimating the worst case stiffness for the fixed-fixed ballscrew application, the minimum stiffness can be found at the middle of the ballscrew and is equal to $3.44x10^6$ *lb/in* in the experimental system.

4.2.2 Ballnut Axial Stiffness.

There are two basic classifications of ballnuts, pre-loaded and non pre-loaded. The pre-loaded ballnut consists of tracks of recirculating balls that run along the thread groove of the ballscrew. Pre-load is established by having the tracks of balls pushed against opposing sides of the ballscrew thread as seen in Figure 4-5.

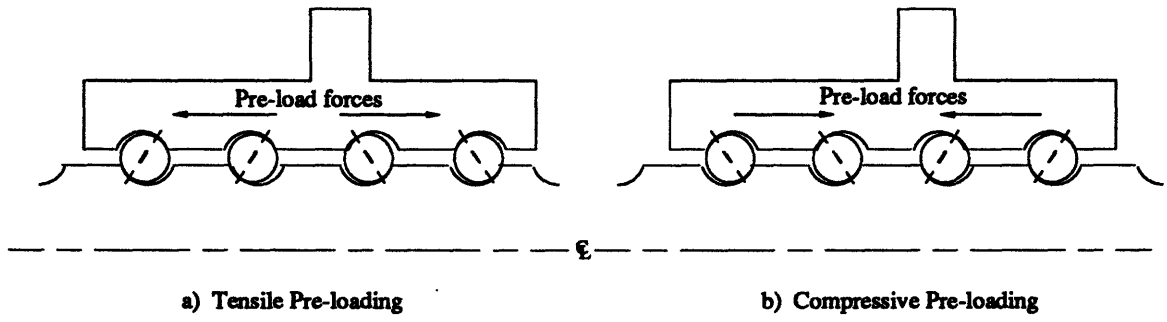

Figure 4-5. Anti-Backlash Ballnut Preloads.

These ballnut pre-loading configurations are termed 'anti-backlash' as they maintain a load on both sides of the ballscrew threads. This minimizes the loss of linear positioning accuracy when the motor changes directions. The pre-load can be created in either the tensile or compressive fashion as seen in Figure 4-5 through the use of spacers, spring washers, or oversized balls. Each process has its advantages and disadvantages and these should be discussed with the ballnut manufacturer when designing an actuator. The tensile pre-loading scheme used in our experimental machine-tool axis allows excellent handling of moment loads about the ballnut due to the effective bearing spread.

The stiffness of the ballnut is derived in much the same way as for the axial stiffness of the angular contact ball bearing. Through geometric considerations one can calculate the pre-load within the system to determine the existing contact angles through the recirculating

balls in the tracks. This leads into the amount of elastic deflection between the thread groove on the ballscrew and the steel balls while loaded axially.

Most catalogs will quote an axial stiffness value that would occur under an axial load that is 30% of the basic dynamic rated load for the ballnut. When the axial load F_a is different than 30% of the basic dynamic load rating for the ballnut, the axial stiffness will change as the contact angle changes across the recirculating balls. To solve for axial stiffnesses resulting from loads that are not equivalent to 30% of the basic dynamic rated load the following equation can be used:

$$S_{ballnut} = 4.57x10^4 \, S \left(\frac{F_a}{0.3 \, C} \right)^{1/3} \qquad 4.9$$

Where S is specified by the manufacturer and is related to the elastic displacement between the screw groove and the steel balls under an axial load of 30% of the basic dynamic load rating for the ballnut. F_a is the axial load, and C is the basic dynamic rated load. $S_{ballnut}$ is delivered in units of lb/in.

The ballnut being used in our application has been manufactured with a minimum stiffness of $5.5x10^6$ *lb/in* when the ballscrew is stretched by 0.0015".

4.3 Ballscrew System Torque.

Torque was introduced in Section 2.3 as a means of evaluating the frictional resistance to rotational motion. The amount of torque necessary to actuate a ballscrew driven carriage can be attained by summing the individual torques of the system components. These are the torques associated with the support bearing, ballnut and ball bushing rolling resistances, as well as the carriage and ballscrew rotational inertias.

For precision applications where torque values are critical, motor and rotary encoder internal torques must be taken into account. However, in our simulation of a manufacturing ballscrew application, the motor and rotary encoder torques are negligible when compared to the torque required to actuate the ballscrew, preloaded support bearings, carriage mass, and ball bushings. The drive torque, or the torque necessary to actuate the

ballscrew axis, will be calculated for constant speed and maximum acceleration conditions. This will be challenged experimentally in Section 5.2.1.

The constant speed drive torque determines not only the constant load on the motor, but can also be used to anticipate the amount of heat energy put into the system. In Section 4.1, temperature effects were shown to be critical in maintaining ballscrew system axial stiffness. The other torque quantity, the drive torque at acceleration, represents the maximum torque required of the motor.

The system torque, T_{system}, for the two motion conditions will be solved by separating the ballscrew system into the influencing components and calculating their individual torque contributions. For motion at constant speed, the start-up inertias of the carriage and ballscrew are neglected. The system torque is a summation of the torques related to: the efficiency of the ballscrew, the ballscrew preload effects on the ballnut torque, and the torques associated with the support bearings.

$$T_{system} = T_{ballscrew} + T_{ballnut} + T_{support\ bearings} \qquad 4.10$$

Equation 4.10 is in units of in-lb. In addition to the system torque associated with constant speed operation, there are torque components related to the acceleration of the carriage and ballscrew masses. In order for the system to start moving, the rotational inertias of the ballscrew and the reflected carriage load must be overcome. The reflected carriage load is used to represent the equivalent rotational inertia of the carriage system as its movement is linear.

The maximum torque required to accelerate the axis is as follows:

$$T_{maximum} = T_{system} + \left(J_{motor} + J_{ballscrew} + J_{carriage}\right)\frac{\omega}{386\ t_a} \qquad 4.11$$

T_{system} is obtained through Equation 4.10. J_{motor} is available from the motor manufacturer and the rotational inertias for the ballscrew and the reflected carriage load can be found in Sections 4.3.4 and 4.3.5. The acceleration time t_a is the desired time for the axis to accelerate from a standstill to the desired velocity. Located in the denominator on the right-hand side of Equation 4.11 is the acceleration due to gravity (386 in/sec^2) and the angular velocity, ω, of the axis is in units of rad/sec and can be solved through Equation 4.12.

$$\omega = \frac{2\pi V}{p} \qquad 4.12$$

V is the desired linear velocity in units of in/sec and p represents the lead of the ballscrew in inches.

Using Sections 4.3.1-4.3.5 to compute the various component torques, the following table of values arises from Equations 4.10 and 4.11 summarizing the theoretical start-up and constant speed torque values.

	ballscrew axis with ACBBs	ballscrew axis with TRBs
left end support bearings	3(2.08) = 6.24 in-lb	2(10.67) = 21.34 in-lb
right end support bearings	6.24 in-lb	21.34 in-lb
ballnut torque	18.0 in-lb	18.0 in-lb
torque due to guideways and carriage	12.0 in-lb	12.0 in-lb
constant speed torque	42.48 in-lb	72.68 in-lb
torque due to acceleration	9.17 in-lb	9.17 in-lb
maximum torque	51.65 in-lb	81.85 in-lb

4.3.1 Ballscrew Torque at Constant Speed.

Ballscrews converting rotary motion into linear motion at constant speed demonstrate torque values related to the load on the system F, the lead of the ballscrew p, and the normal ballscrew efficiency e.

$$T_{ballscrew} = \frac{F\,p}{2\pi\,e} + T_c \qquad 4.13$$

$F = \mu W/16$ with $\mu=0.004$ for ball bushing linear guideway systems where W represents the weight of the carriage in lbs while p is representative of the distance between two adjacent threads measured along the axis of the ballscrew. The normal efficiency e can be obtained from the ballscrew manufacturer and is a function of surface finish, thread angle, and operating conditions (typically 0.90~0.95). T_c is a constant representative of the torque due to the frictional motion of all moving elements in the application. The ballscrew torque should be expressed in units of in-lb to be used in conjunction with Equations 4.10 and 4.11.

4.3.2 Ballnut Torque.

The frictional torque associated with a preloaded ballnut is a function of several factors. The geometry of the ballnut and the recirculating balls as well as the lubrication scheme and ballscrew stretch all contribute to the torque contribution of the ballnut assembly. The ballnut manufacturer can quote an accurate value based upon system characteristics for use in Equations 4.10 and 4.11. For the machine-tool application under consideration in Section 5, the maximum ballnut torque is rated at 18.0 in-lb.

4.3.3 Support Bearing Torque.

The torque associated with the ballscrew support bearings can be found in Sections 2.2 and 3.2 depending upon which type of bearing is being used. Remember that the torque values of each of the bearings must be calculated separately as some of the bearings are operating under different loads. The support bearing torque is the sum of the torques associated with all of the bearing rows employed on the axis.

4.3.4 Ballscrew Rotational Inertia.

The rotational inertia of the ballscrew is found by approximating the ballscrew as a cylindrical mass. When applied to the ballscrew the following equation results:

$$J_{ballscrew} = \frac{\pi \rho D^4 Z}{32} \qquad 4.14$$

ρ is the material density in lb/in^3, D is the diameter of the base of the thread groove on the ballscrew in inches, and Z is the total length of the ballscrew in inches.

4.3.5 Effective Carriage Rotational Inertia.

The rotational inertia imposed on the ballscrew system by the carriage can be found through the following relationship:

$$J_{carriage} = \frac{W}{e}\left(\frac{p}{2\pi}\right)^2 \qquad 4.15$$

W represents the weight of the carriage in lbs, *e* is the ballscrew efficiency, and *p* is the lead of the ballscrew in inches.

4.3.6 Ballscrew System Life

Many calculation procedures exist for computing the lives of machine-tool components. However, due to the variability of life calculations between manufacturers as a result of their unique design criteria and manufacturing processes, this section will not detail the actual life calculations of bearings or ballscrews. Instead, a relative life approach will be used referencing as an example the experimental machine-tool axis, discussed in greater detail in Section 5.

The operating life of a system is described by the component with the shortest life span. Life values of the bearings and the ballscrew used in the experimental machine-tool axis have been computed using the manufacturer's catalogs. The operating life of the bearings was then transformed into inches of travel as this is the most commonly used rating for ballscrews. This requires knowing the lead of the ballscrew and the life rating in hours (L_{10}) of the bearings.

	Life (inches of travel)
angular contact ball bearing	10^8
tapered roller bearing	10^8
ballscrew	10^6

The bearing life calculations were based upon average operating conditions for the ballscrew application. From the above estimated life values, it is apparent that the ballscrew represents the 'shortest-life' component and will need replacing before the bearings. When the ballscrew begins to show signs of wear that are detrimental to performance, it is wise to replace both ballscrew and support bearings. Brinneling of the bearings has been known to occur during lackluster assembly and disassembly procedures and may not be obvious until the machine is running out of precision or fails prematurely. Machine down-time is expensive as are labor hours invested in repetitive rebuild operations.

5.0

Ballscrew System Evaluation.

With the interest of comparing the operation of the tapered roller bearing to the angular contact ball bearing, a machine-tool axis was constructed. In Sections 2 and 3 the different bearings were evaluated outside of the ballscrew application while this section serves to document the performance of the angular contact ball bearings and tapered roller bearings in the machine-tool application. Included is the design of the test rig, the testing procedures and the findings of the bearing comparisons.

5.1 Experimental Machine-Tool Axis.

The test rig constructed to evaluate the ballscrew support bearing performance can be seen schematically in Figures 5-1 and 5-2.

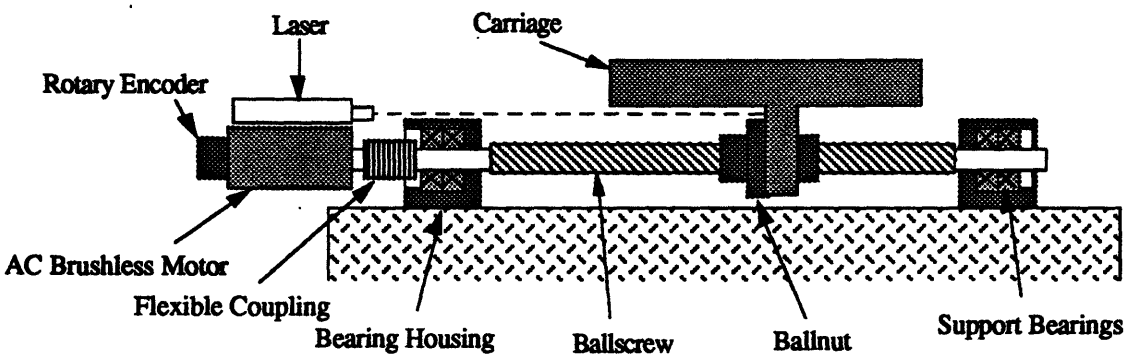

Figure 5-1. Experimental Machine-Tool Axis Setup.

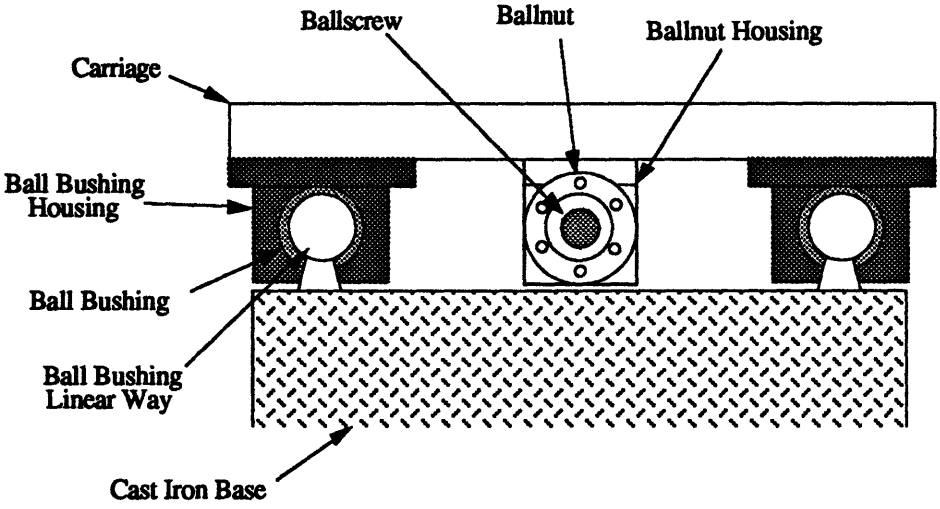

Figure 5-2. End-view of the Experimental Machine-Tool Axis.

This test setup was designed to study the effects the different support bearing packages would have on the system. In any precision ballscrew driven axis, the issues of stiffness and torque are critical. Too little stiffness creates a compliant system unable to deliver accuracy, repeatability, or controllability. Too much torque requires larger, more costly drive systems, extra lubrication subsystems, and exposes the axis to temperature induced thermal strains.

By creating an accepted standard of current machine-tool capabilities, the tests were aimed at demonstrating the effectiveness of the tapered roller bearing as a ballscrew support bearing.

A precision ballscrew was purchased that would accurately represent the state of the art in ballscrew capabilities. The ballscrew had an operating stroke of over 30" and a supported length of approximately 52". Designed to accommodate a rapid traverse rate of 800ipm, the maximum diameter of the screw was 45mm while the diameter of the bottom of the thread groove was 35mm. The lead on the ballscrew was listed as 14mm but was ground slightly short of this mark to accommodate the stretch that would be placed on the ballscrew. The stretch corresponded to 0.0015" over the supported length for a thermal compensation of just under 5°F (Refer to Section 4.1).

The shoulder on the ballscrew has been ground to fixture 35mm bore support bearings. Commonly used on this particular ballscrew are the MM35BS72 triplex angular contact ball bearings manufactured by the Fafnir-Torrington Company. These bearings have a width of 15mm and an outside diameter of 72mm. The triplex angular contact ball bearing envelope was used as a constraint in the design of the prototype tapered roller bearing to be manufactured by The Timken Company.

Driving the ballscrew system is a Siemens AC Brushless Servomotor rated for 2000 rpm and 159 in-lb of continuous torque. Operating via current command from the motor manufacturer's drive amplifier, an external PC based single-axis controller from Aerotech was responsible for the actuation commands. Wanting to construct the experimental axis to mimic manufacturing applications as much as possible, a Heidenhain rotary encoder was mounted to an extension shaft off the back of the motor and used to provide the position and velocity feedback information to the controller. The encoder supplied 10,000 counts per revolution which was increased to 40,000 with a 4x interpolation. Coupled with the lead of the ballscrew, this allowed a theoretical controllable resolution of 14μin per count.

An open style ball bushing system from Thomson was used to support the carriage. The ball bushings offer constraint in 5 directions with the unconstrained direction falling in the direction of the ballscrew. As the ballscrew is only supposed to experience thrust loads as a result of the motor attempting to advance the threads through the non-rotating ballnut, the ball bushings are responsible for absorbing all non-axis components of the loads. The ball

bushings have several tracks of recirculating balls that are preloaded against the cylindrical ways, causing them to roll over the way surface with minimal slip.

5.2 Testing.

This section deals with the tests used to evaluate the performance of the experimental machine-tool axis using the different ballscrew support bearings. The angular contact ball bearings and the tapered roller bearings were mounted in triplex and two-row-direct fashion respectively. The information gathered from the following tests will determine the feasibility of the two-row tapered roller bearing as a cost effective alternative to the triplex angular contact ball bearing. Four system evaluations were performed:

- *Startup and Constant Velocity Torque Measurement*
- *Vibration Analysis*
- *Accuracy and Repeatability Study*
- *Operating Temperature*

The test procedures and resulting data for the above evaluations can be found in Sections 5.2.1-5.2.4. When appropriate, the values resulting from the theoretical approximations presented in this paper will be evaluated along-side the experimental values.

5.2.1 Torque Tests.

Using a torque wrench, the start-up and constant velocity torque of the experimental machine-tool axis was verified. The following table summarizes the theoretical predictions and the experimental values for both the angular contact ball bearing and tapered roller bearing systems:

	theoretical predictions		experimental values	
	start-up torque	constant speed torque	start-up torque	constant speed torque
ACBB system	51.65 in-lb	42.48 in-lb	51 in-lb	47 in-lb
TRB system	81.85 in-lb	72.68 in-lb	80 in-lb	75 in-lb

The theoretical values correlate well with the experimental values taken from the test rig.

The theoretical predictions do not take into account the torque components that result from slight misalignments between the ballscrew and the ball bushing linear ways. The set-up procedure for the ballscrew axis calls for a maximum allowable misalignment of ±0.002" over the length of the ballscrew travel. This misalignment is measured relative to the fixed ball bushing guideway. When assembling the ballscrew axis it is suggested that the ballscrew be hand driven using a torque wrench over the length of ballscrew travel. During this process, incremental positioning and tightening of the support housings is required to improve the ballscrew alignment and attain a minimum torque reading. If the ballscrew is misaligned, premature wear patterns will develop resulting in reduced accuracy and shortened life.

In Section 5.2.4 the effects of the differing bearing package torques will be seen in their effects on the operating temperature. With the 159 in-lb motor, the relative torque capacity used with the angular contact ball bearing arrangement was 32% compared to 50% for the tapered roller bearing solution.

5.2.2 Vibration Analysis.

In Sections 2.1 and 3.1 methods were presented for calculating the axial stiffnesses of the support bearings in a ballscrew axis. This information was incorporated into the stiffness calculations for the ballscrew system presented in Section 4.2. It is the purpose of the vibration analysis to challenge the theoretical system stiffness calculations experimentally.

To discern the ballscrew system stiffness, a simple impact test was arranged to monitor the amount of signal transmission through the system. By observing the response of the static system to a known input, a fair approximation could be made of the system stiffness.

The tests incorporated an accelerometer, impact hammer, and a two channel digital signal analyzer. The servomotor was removed and the carriage was placed at the center of the ballscrew to simulate the most compliant arrangement for the fixed-fixed ballscrew. An accelerometer was epoxied to the motor end of the ballscrew and the impact hammer was used to distribute a blow to the tail end of the ballscrew. The digital signal analyzer recorded the signals from the impact hammer (mV/lbf) and accelerometer (mV/g), performed a double integration on the accelerometer signal, to produce a transfer function relating the system compliance in units of in/lb. The inverse of the largest peak represents

the lowest stiffness value and is used to determine system stiffness. Figures 5-3 and 5-4 show two sample outputs from the impact tests.

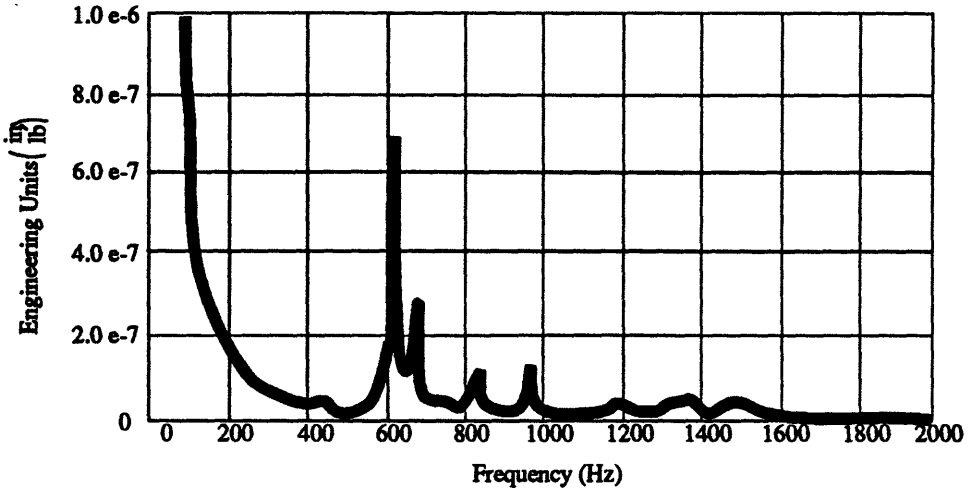

Figure 5-3. Impact Vibration Data - Ballscrew Axis - Angular Contact Ball Bearings.

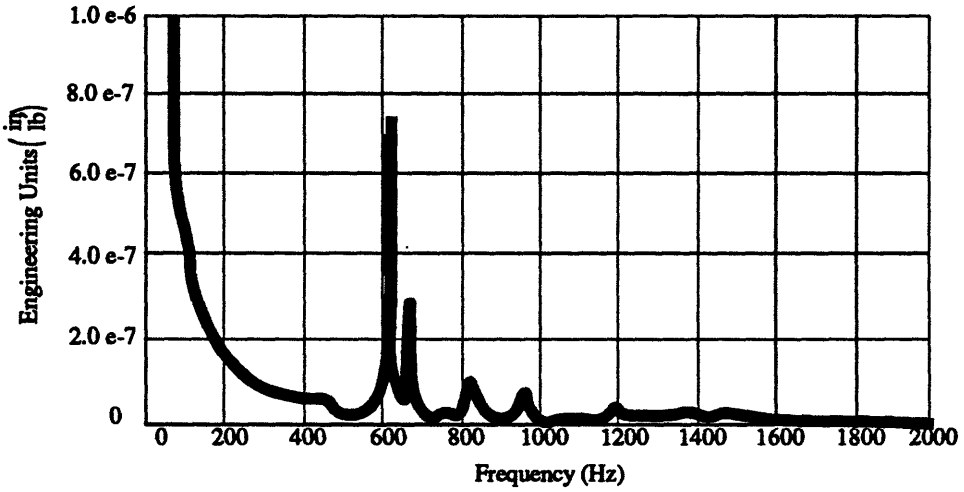

Figure 5-4. Impact Vibration Data - Ballscrew Axis - Tapered Roller Bearings.

The theoretical stiffness values can be seen below compared against the experimental values from Figures 5-3 and 5-4:

	Theoretical Ballscrew System Stiffness	Experimental Ballscrew System Stiffness
Angular Contact Ball Bearings	1.48×10^6 lb/in	1.439×10^6 lb/in
Tapered Roller Bearings	1.33×10^6 lb/in	1.355×10^6 lb/in

The theory presented through Sections 2.1, 3.1, and 4.2 have come within ±2.5% of the experimentally defined system stiffness values. There is only a 6% difference in system stiffness when using either support bearing package. This demonstrates the cost effectiveness of the tapered roller bearing in providing axial stiffness for ballscrew driven systems.

5.2.3 Accuracy and Repeatability Analysis.

Following the ASME.B5 standard[1] for the performance evaluation of numerically controlled machining centers, the linear positioning accuracy and repeatability of the experimental machine-tool axis was verified. Both the triplex angular contact ball bearings and the tapered roller bearings were evaluated in their role as the support bearings in the ballscrew axis. To develop a fair comparison between the different bearings, the motion control-loop settings, ballscrew stretch, and operating conditions were held constant. This eliminated any control-loop tuning bias such that a head-to-head comparison could be made. A laser was used to measure the accuracy and repeatability of the axial location of the ballnut during the tests.

Linear Displacement Accuracy for an Axis

The following procedure follows from section 5.5.2.6 of the ASME.B5.54 standards.

The 30" travel length of the ballscrew was divided into ten intervals defining eleven points. The motion controller was programmed to start at zero and advance along the axis at a rapid traverse speed of 800 ipm, stopping and dwelling for a few seconds at each point while the laser acquired position data. The corrected laser reading (thermally compensated laser readout) was subtracted from the corrected machine reading (where we want the ballnut according to the motion program) at the stopping points along the axis. The axis was cycled back and forth in this move-stop-dwell-datalog fashion while the data was averaged

---

[1] B5.54 Methods for Performance Evaluation of Computer Numerically Controlled Machining Centers. Copyright ASME (1993)

for each point in each direction. The results can be seen graphically in the following plots showing the positioning error along the axis in each direction.

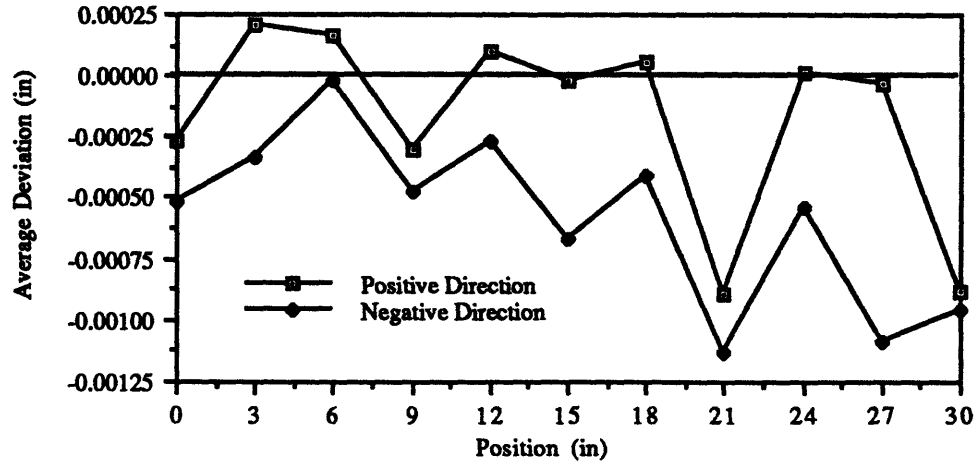

Figure 5-5. Machine-Tool Axis Positioning Accuracy Data using Angular Contact Ball Bearings.

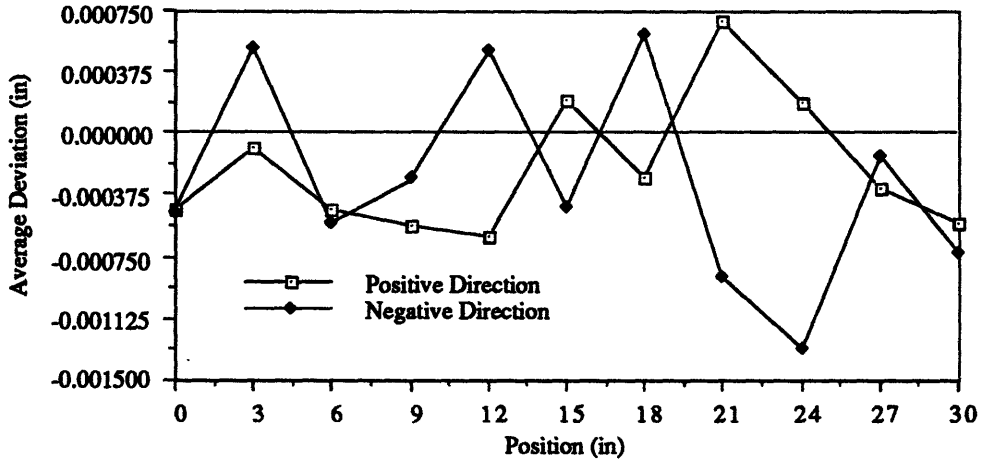

Figure 5-6. Machine-Tool Axis Positioning Accuracy Data using Tapered Roller Bearings.

Three sets of bi-directional moves were averaged to create the two lines seen in each of the above plots. The linear displacement accuracy of the axis is defined as the total range of the two sets of average deviations in the figures. An additional performance error can also be

obtained from the above plots. The maximum reversal error is the largest range of the averaged forward and reverse readings at any point along the axis.

The positive direction in Figures 5-5 and 5-6 is defined as the direction moving away from the motor. The ballscrew system when using the angular contact ball bearings shows a linear displacement accuracy of ±0.000688" with a maximum reversal error of ±0.00054". When the tapered roller bearings were used, the linear displacement accuracy was similar at ±0.000751 while the maximum reversal error was ±0.00078" A large amount of the error seen in the linear displacement accuracy of the machine-tool axis can be minimized through tighter tuning of the positioning control loop which involves adjustments of the various gains within the feedback loop. In doing so, the positioning capability of the machine-tool will be optimized, however, it is not the purpose of this paper to define control loop standards.

An 'average-performance' control loop was established and the conditions maintained for both bearing tests such that a head-to-head comparison could be made between the use of the different bearing packages. The overall goal was to demonstrate that the tapered roller bearings could deliver similar performance under the same operating conditions as the angular contact ball bearings.

By using the same control scheme for both bearing units as well as identical dwell times before capturing displacement information, the true positioning potential of the axis was not realized. This was avoided in light of the desire for a comparative analysis as opposed to an optimization. It should be noted that when given ample time to dwell during the motion program, the displacement accuracies for both bearing sets were improved by roughly an order of magnitude.

Bi-Directional Repeatability for an Axis

The following procedure was taken from section 5.5.2.8 of the ASME.B5.54 standards.

The bi-directional repeatability is evaluated as the ability of the machine to return to nominally the same point. The following procedure is carried out at both 1/4 and 3/4 of the machine-tool axis' travel length. The traverse rate is set at approximately 6ipm and a motion program is used that moves the ballnut 6mm in the positive direction, then returns

to the original position and the laser value is recorded. It is next moved 6mm in the negative direction and returned to its original position, where again the laser is read. This is repeated for a total of ten trials and the data is gathered and analyzed to determine the amount of bi-directional repeatability present within the system. The working tolerance for bi-directional repeatability is the maximum range of the data gathered at either position along the ballscrew.

The angular contact ball bearings showed a bi-directional repeatability of ±0.0019" while the tapered roller bearings registered ±0.0011".

Again, the control loop schemes and dwell times before sampling were held constant for both series of bearings for the comparative reasons detailed in the previous section on linear displacement accuracy.

5.2.4 Operating Temperature.

A duty cycle was created for the machine-tool axis to monitor the change in temperature of the ballscrew support bearing packages and the ballnut. The carriage was cycled back and forth along the full length of travel (30") operating at 1/4 of the rapid traverse speed (=200ipm) with a dwell of 5 seconds on either end of the stroke. One-fourth of the rapid traverse speed was chosen as it is more likely that a machine of this nature will spend the majority of its time performing feed cuts at a fraction of the rapid traverse speed.

Thermocouples were placed on the ballnut and the motor side bearing housing. The test was initially run with the angular contact ball bearings as the support bearings and then re-run using the tapered roller bearings. Figure 5-9 displays the results of the 3-hour long tests charting the ballnut and motor-side support bearing temperatures. The ballnut temperature curve was similar for both tests hence only one curve is present in Figure 5-9.

The expected relationship for the heat generation and resulting temperatures of the three components (ballnut, angular contact ball bearings, and tapered roller bearings) stem from rotational resistance. The frictional resistance created can be quantified through the component torque which is directly related to heat generation. Looking at the theoretical torques of the components in the machine-tool axis and comparing these values to the temperature increases of the components during the three hour duty cycle:

	torque (in-lb)	ΔºF
triplex angular contact ball bearing	8.7	6.7
ballnut	18.0	13.0
two-row tapered roller bearing	28.0	19.6

The temperature increases during the tests were seen to be related to the ratios of the component torques. These ratios are not exact due to a number of factors. Heat generation by the ballnut is spread out over a much larger dissipative surface (30" of ballscrew travel length) while the bearings are heating a much more localized envelope. Also, the rib-roller contact areas for the tapered roller bearings are aligned such that they are next to each other (refer to direct mounting figures in Section 3) creating two adjacent heat sources, slowing dissipation.

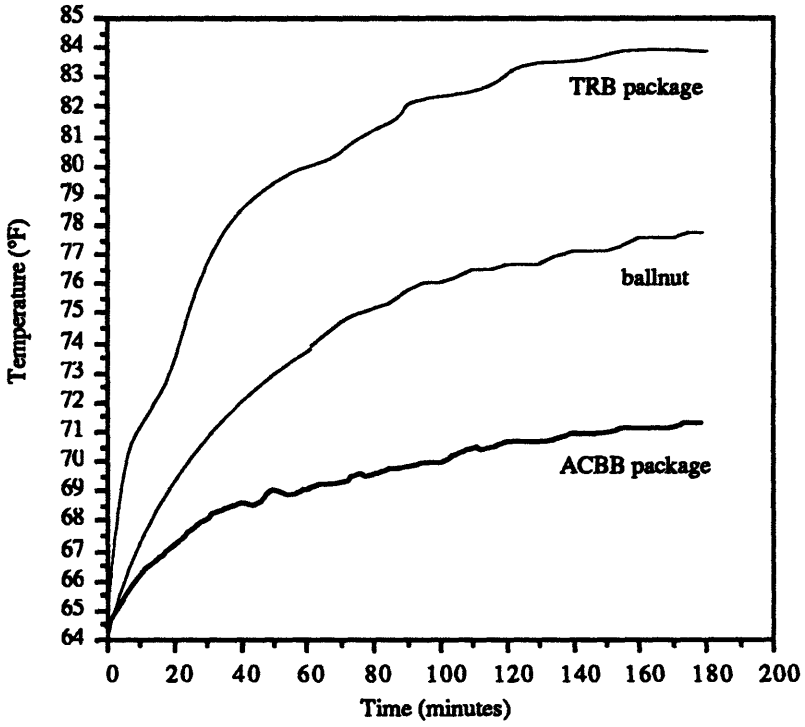

Figure 5-9. Comparison of Ballnut and Support Bearing Temperatures.

The tapered roller bearings performed as expected. With a larger torque, the bearings will run hotter. This characteristic can be critical in precision applications but can be assuaged through modified rib-roller designs, surface finishes, and lubrication schemes.

5.3 Discussion of Results.

The results detailed in Sections 5.2.1-5.2.4 offer a comparative analysis between the two types of bearings and their respective mounting configurations. The machine-tool ballscrew application is concerned with maintaining axial stiffness while minimizing heat generation such that positioning accuracy can be maintained. It was shown that working within the same volume, four tapered roller bearings (two per ballscrew end) could provide axial stiffness values similar to those observed when using six angular contact ball bearings (3 per ballscrew end). The stiffness difference when incorporated into the machine-tool axis was very small and attributable in part to gauging limitations.

The row for row torque disparity of nearly four times between the tapered roller bearing and angular contact ball bearing under application conditions is of serious concern for most machine-tool applications. However, the tapered roller bearings use only 2/3 as many rows in their support package design bringing the relative torque disparity down to 2.67 times that of the angular contact ball bearing package. As Section 5.2.4 verified, the temperature rise of the tapered roller bearing package was on the order of the torque disparity, roughly three times that of the angular contact ball bearing package.

The results as seen in the previous sections offer great insight into the potential of the tapered roller bearing in ballscrew support applications. It would appear that the tapered roller bearing is tailor made for applications that can be described by the following characteristics:

- Low speed (< 250 sfpm at the rib)
- Intermittent use or appreciable dwell periods
- High load carrying capability
- High stiffness requirements
- Stiffness stability throughout loading range
- Small motion applications
- Suspended or cantilevered loads
- Minimum number of rows

Until improvements are made in the rib-roller interface of the tapered roller bearing, the high volume, precision machine-tool market may remain out of reach. The deciding factors for these particular applications will stem from the machine-tool manufacturer's ability to account for the thermal effects on the machine and the trade-offs therein.

A design alternative does exist using the same tapered roller bearing that would cut the torque considerably. Returning to Section 3.1 and the linear load deflection curve of the tapered roller bearing, it would be feasible to lessen the amount of preload on the bearing. In doing so the amount of torque require to operate the bearing would be reduced which would lower the amount of heat generation and improve the operating temperature. Refering to Figure 3-13 where torque is compared against axial load, it can be seen that if the preload is lowered to 750 lbs axially across each of the bearings in the two-row stack-up, the torque per bearing row is significantly less. Charting the loads across each of the four support bearings for the 1500 lb preloaded system and for a 750 lb preloaded system:

	TRB with 750 lb preload		TRB with 1500 lb preload	
	ballscrew left end	ballscrew right end	ballscrew left end	ballscrew right end
preload condition	750,750	750,750	1500,1500	1500,1500
after ballscrew stretch	105,1395	1395,105	855,2145	2145,855
torque per row	1.5,13.5	13.5,1.5	13.5,14.5	22.0,6.0
total torque	15.0	15.0	28.0	28.0

The dramatic decrease in torque will improve the operating temperature of the bearing package. If the proportionality seen in Section 5.2.4 holds between the package bearing torque and the operating temperature, the 750 lb preloaded system would see a temperature rise on the order of 11°F as opposed to nearly 20°F for the 1500 lb preloaded system.

Of course there is a load carrying tradeoff that occurs. Looking at the 750 lb preloaded arrangement above, after the 1290 lb stretch is applied to the ballscrew, the outermost bearings are seated with only 105 lbs of axial load. Therefore, if perfect load sharing holds, any external load in excess of 210 lbs will unseat one of these bearings depending upon the loading direction.

This example emphasizes the flexibility of system design and the tradeoffs therein. By improving the torque characteristics of the system, the load carrying capacity of the system was put at risk. There are certain application dependent operating conditions that can make or break a machine design, physically and economically. The ability to recognize and take advantage of the inherent strengths and weaknesses of components separates the good designs from the great designs.

6.0

Conclusion.

The tapered roller bearings delivered a cost-competitive solution hindered only by the innate tapered roller bearing characteristic of higher torque and subsequent heat generation. Even so, the tapered roller bearing appears a viable contender for cost effective, high stiffness, slow speed ballscrew applications. This section offers possibilities for future design efforts which could present the tapered roller bearing with volumes of new market potential.

6.1 Recommendations.

For the tapered roller bearing to gain ground in the ballscrew support market, the running torque induced by the sliding friction at the rib-roller end needs to be addressed. Several design options exist for further exploration with steep angle tapered roller bearings including:

- Crowned rib surfaces to control deformation
- Roller large-end optimization
- Improvement of rib-roller contact location
- Roller, raceway, and rib finishes
- Rib lubrication techniques

These areas should be looked into to determine the practical and cost-effective limitations for ballscrew support applications In doing so, potential designs could be accurately evaluated before committing large quantities of time and resources to prototyping and testing. The design limitations study for the ballscrew market should also encompass the possibility of using full compliments of rollers or polymer cages. This would maximize the axial stiffness and load carrying capacity of the bearing and be used in applications such as creep-feed grinders and infeed tables where speed is minimal.

The roller screw market is another area in which the tapered roller bearing would likely flourish. Roller screws are similar to ballscrews in that they transmit rotational motion into linear motion. However, several constrained threads are used in contact along the axis of the screw to operate as the ballnut in the ballscrew application. The large contact area that is formed by the multitude of threads in contact makes this component appreciably stiffer than ballscrews of identical size. These applications are limited in speed as noise and vibratory concerns come into play. They are commonly used in low-speed,intermittent use, high stiffness applications which could benefit from the use of tapered roller bearings as the support bearings on the main screw shaft.

Probably the biggest obstacle in the way of the tapered roller bearings acceptance into the ballscrew support arena lies in the past. Improvements in design and manufacturing over the last few decades warrant a fresh look at the possibilities.